IS-T-727

INTERDIFFUSION IN THE Er_2O_3-HfO_2 SYSTEM

William Francis Schiavi

M. S. Thesis Submitted to Iowa State University

Ames Laboratory, ERDA
Iowa State University
Ames, Iowa 50011

Date Transmitted: October 1976

NOTICE

This report was prepared as an account of work sponsored by the United States Government. Neither the United States nor the United States Energy Research and Development Administration, nor any of their employees, nor any of their contractors, subcontractors, or their employees, makes any warranty, express or implied, or assumes any legal liability or responsibility for the accuracy, completeness or usefulness of any information, apparatus, product or process disclosed, or represents that its use would not infringe privately owned rights.

PREPARED FOR THE U. S. ENERGY RESEARCH AND DEVELOPMENT ADMINISTRATION UNDER CONTRACT NO. W-7405-eng-82

MASTER

DISTRIBUTION OF THIS DOCUMENT IS UNLIMITED

DISCLAIMER

This report was prepared as an account of work sponsored by an agency of the United States Government. Neither the United States Government nor any agency Thereof, nor any of their employees, makes any warranty, express or implied, or assumes any legal liability or responsibility for the accuracy, completeness, or usefulness of any information, apparatus, product, or process disclosed, or represents that its use would not infringe privately owned rights. Reference herein to any specific commercial product, process, or service by trade name, trademark, manufacturer, or otherwise does not necessarily constitute or imply its endorsement, recommendation, or favoring by the United States Government or any agency thereof. The views and opinions of authors expressed herein do not necessarily state or reflect those of the United States Government or any agency thereof.

DISCLAIMER

Portions of this document may be illegible in electronic image products. Images are produced from the best available original document.

NOTICE

This report was prepared as an account of work sponsored by the United States Government. Neither the United States nor the United States Energy Research and Development Administration, nor any of their employees, nor any of their contractors, subcontractors, or their employees, makes any warranty, express or implied, or assumes any legal liability or responsibility for the accuracy, completeness, or usefulness of any information, apparatus, product or process disclosed, or represents that its use would not infringe privately owned rights.

Available from: National Technical Information Service
U. S. Department of Commerce
P.O. Box 1553
Springfield, VA 22161

Price: Microfiche $2.25

IS-T-727

Interdiffusion in the Er_2O_3-HfO_2 System

by

William Francis Schiavi

A Thesis Submitted to the
Graduate Faculty in Partial Fulfillment of
The Requirements for the Degree of
MASTER OF SCIENCE

Department: Materials Science and Engineering
Major: Ceramic Engineering

Approved:

In Charge of Major Work

For the Major Department

For the Graduate College

Iowa State University
Ames, Iowa

1976

TABLE OF CONTENTS

INTRODUCTION

The purpose of this thesis work is to study interdiffusion in the Er_2O_3-HfO_2 system. This study is part of the continuing effort at the Ames Laboratory ERDA to describe atomic movement in fluorite type ceramic materials.

The Er_2O_3-HfO_2 system was studied in detail by Johnstone (1970). Figure 1 is his proposed phase diagram. Compositions consisting of less than 10 mole % Er_2O_3 are mixtures of monoclinic (M), tetragonal (T), and fluorite (F) solid solutions. The monoclinic⇄tetragonal polymorphic transformation in this composition range is accompanied by a destructive volume change which renders these materials very troublesome in any application where dimensional stability and sample integrity must be maintained. This very high-HfO_2 region of the system is not investigated in this study.

At concentrations in the range from 10 to 50 mole % Er_2O_3 a continuous series of fluorite (F) solid solutions exist. This structure is stable through the temperature range 1600°-1800°C where the destructive M⇄T polymorphic transformation occurs in material of lower Er_2O_3 concentrations. Rare earth oxide stabilized HfO_2 is important to ceramists for its potential high temperature applications (Schieltz, Patterson, and Wilder, 1971). Johnstone (1970) measured melting temperatures in pure HfO_2 as high as 2825°C with no significant reduction at Er_2O_3 contents up to 30 mole percent. HfO_2 can be stabil-

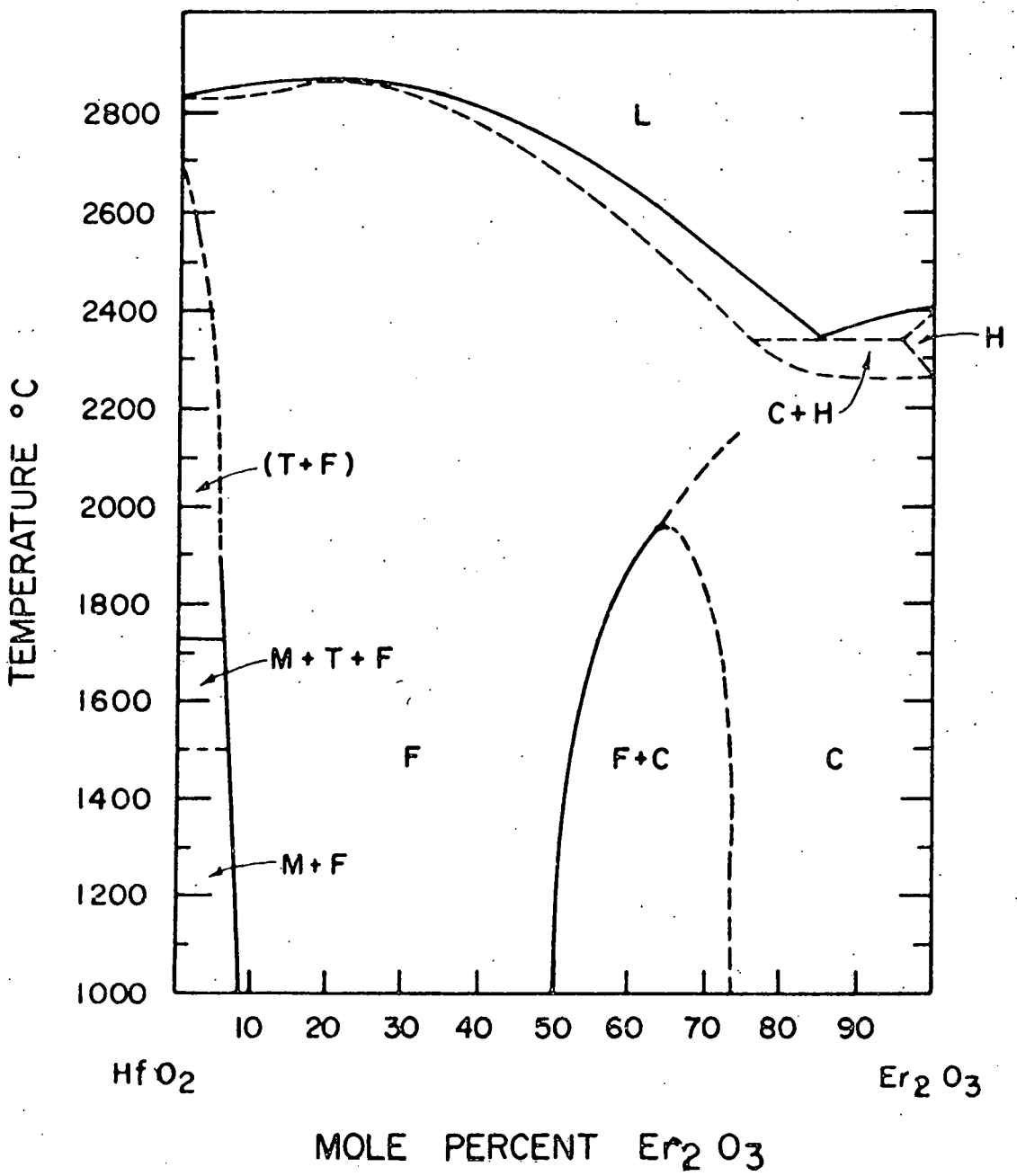

Figure 1. Proposed phase diagram for the HfO_2-Er_2O_3 system (Johnstone, 1970)

ized with CaO, Y_2O_3, or the rare earth oxides and it is reported to be more resistant to progressive destabilization than is the chemically analogous and widely used stabilized ZrO_2 (Curtis, Doney, and Johnson, 1954, Buckley, 1969). Buckley and Wilder (1969) reported that Y_2O_3-stabilized HfO_2 is more stable than CaO or MgO-stabilized HfO_2. Hf has a high thermal neutron absorption cross section (approximately 100 barns) and by resonance capture, it also absorbs epithermal neutrons. The rare earth oxides would appear to be ideal stabilizers for HfO_2 in nuclear applications since, as a group, the rare earths oxides have good thermal stability and an extreme range of thermal neutron capture cross sections.

The forementioned applications for stabilized hafnia may someday be very important, but are cited here principally for background information. The F solid solutions are of interest to this study mainly because the fluorite structure may be thought of as the parent structure from which the C-type rare earth oxide structure of pure Er_2O_3 is derived. The fluorite structure is a cubic arrangement in which the cations form a face centered cubic array, each cation in eight-fold coordination with oxygen anion sites that in turn form a simple cubic anion site lattice. Johnstone (1970) determined that as Er_2O_3 dissolves into Er_2O_3-stabilized HfO_2, anion vacancies are formed in the fluorite structure according to the equation:

$$Er_2O_3(s) \rightleftarrows 2Er'_{Hf} + 3O_o + V_o^{\cdot\cdot} \qquad (1)$$

In Equation 1, the standard Kroeger-Vink notation has been used, that is:

Er'_{Hf} is an Er+3 cation on a Hf+4 site

O_o is an O^{-2} anion on an O^{-2} site

$V_o^{\cdot\cdot}$ is a vacant O^{-2} site

' indicates a -1 charge

$^{\cdot\cdot}$ indicates a +2 charge

Each ion in the Er_2O_3-stabilized HfO_2 fluorite structure is displaced slightly from its ideal location depending on the O^{-2} vacancy concentration. The unit cell for this structure is the basic fluorite unit composed of four $Hf_{1-x}Er_xO_{2-(x/2)}$ formula units. Other ceramic materials possessing the fluorite structure, in addition to stabilized HfO_2 and ZrO_2, include the alkaline earth fluorides and the actinide oxide fuels UO_2, PuO_2, ThO_2 and UO_2-PuO_2 solid solutions.

In Figure 1, the region of greatest importance to this study is that below 2000°C in temperature and greater than 75 mole % Er_2O_3 in concentration. Compositions in this range are all solid solutions of the C-type rare earth oxide structure. As noted previously, this structure may be thought of as a derivative of the fluorite structure. The cations form the expected face centered cubic array, each slightly displaced from its ideal FCC position. In pure Er_2O_3, the cations are each coordinated with 6 anions which occupy 3/4 of the corner sites of an eight-member simple cubic anion cube. The O^{-2}

anions form a simple cubic array with empty anion sites ordered such that a C-type unit cell contains eight modified fluorite subunits, or 16 formula units of Er_2O_3. It is assumed by analogy with other fluorite structure ceramics that the predominating intrinsic defects in pure Er_2O_3 are anion Frenkel pairs. It is well established (Franklin, 1968) that anion Frenkel pairs predominate in CaF_2. Electrical conductivity studies in nonstoichiometric rare-earth oxides (Macki, 1968; Schieltz et al., 1971) have reported the existence of oxygen interstitials in oxygen-rich oxides and oxygen vacancies in oxygen-deficient oxides. It is therefore reasonable that at stoichiometry both oxygen interstitials and oxygen vacancies exist in equilibrium, that is, as anion Frenkel pairs.

According to Johnstone (1970), HfO_2 solution into Er_2O_3 is characterized by the formation of anion interstitials. As Hf^{+4} cations randomly enter Er^{+3} sites, the extra O^{-2} anions take up "interstitial sites" which are probably the normally-unoccupied anion sites of the C-type rare earth oxide structure. This solution process is described by the following equation, where once again the Kroeger-Vink notation has been used:

$$HfO_2(s) \rightleftarrows Hf_{Er}^{\cdot} + 3/2\ O_o + 1/2\ O_i'' \qquad (2)$$

The symbol O_i'' represents one oxygen "interstitial" with a -2 charge. This dissolving of HfO_2 into Er_2O_3 begins to random-

ize the location of unoccupied anion sites by inserting O^{-2} anions into some of those previously unoccupied sites. As more HfO_2 is dissolved, this randomization continues and the C-type structure gradually approaches the fluorite structure. At some critical HfO_2 concentration between 25 mole % and 50 mole %, complete randomization of empty anion sites occurs spontaneously and the fluorite structure is the result. The reverse transformation results as Er_2O_3 is added to Er_2O_3-stabilized HfO_2, that is, the fluorite structure changes toward the C-type structure.

Atomic movement in the fluorite structure and related ceramic materials has been studied extensively at the Ames Laboratory. Berard (1971) examined cation tracer self-diffusion in single crystal CaF_2 and earlier in polycrystalline Er_2O_3 and Y_2O_3 (Berard and Wilder, 1969). Berard, Wirkus and Wilder (1968) and Basler and Berard (1974) studied O^{-2} self-diffusion in single crystal Er_2O_3 and other C-type rare earth oxides. Interdiffusion was investigated in single crystal alkaline earth fluoride systems, namely, CaF_2-SrF_2 (Scheidecker and Berard, 1973), YF_3-CaF_2 (Visser, Schiavi, and Berard, 1975) and SrF_2-BaF_2 (Scheidecker and Berard, 1976). Interdiffusion in the polycrystalline rare earth oxide systems Er_2O_3-Y_2O_3 and Er_2O_3-Ho_2O_3 was studied by Gessel (1971).
The fluorite and rare earth type C structures are favorable to rapid anion movement (Berard et al., 1968; Matzke, 1970) and

one should expect that $D_{anion} >>> D_{cation}$. This characteristic is unusual in ceramics, but is in fact amply verified (Berard, 1971; Berard and Wilder, 1969; Matzke, 1970; Rhodes and Carter, 1966; Simpson and Carter, 1966; Berard, Wirkus, and Wilder, 1968).

This work examines interdiffusion between Er_2O_3 and HfO_2 in Er_2O_3-rich solid solutions having the C-type rare earth oxide structure. It also attempts to extract information on the relative mobilities of Hf^{+4} and Er^{+3} cations in these solutions. Finally it will yield an estimate of the self-diffusion coefficient of Hf^{+4} in essentially pure Er_2O_3.

THEORY OF DIFFUSION IN HfO_2-DOPED Er_2O_3

Diffusion in a solid occurs through the thermally activated random motion of the atoms in the solid matrix. If a potential gradient is imposed across the solid, a material flux will occur in order to reduce the gradient. The gradient may be chemical, electrical, or thermal in nature, but in this study it has been restricted experimentally to chemical only; in other words, there were no externally imposed electric fields or thermal gradients. Atomic movement occurs in three dimensions, but in an isotropic medium, if the gradient is imposed in only one dimension, then only a one-dimensional material flux will be observed. This will be the case studied here.

Fick, as cited in Crank (1956) phenomenologically described the diffusion process in the relation referred to as Fick's First Law:

$$J_i = -D_i \frac{\partial c_i}{\partial X} \tag{3}$$

where J_i is the local flux of diffusing species i, c_i is the local concentration of that species in particles per unit volume, X is the spatial coordinate in the direction of diffusion, and D_i is a proportionality constant called the diffusion coefficient. In this study, Fick's First Law is applied such that Equation 3 becomes

$$J_i = -\tilde{D} \frac{\partial c_i}{\partial X} \tag{4}$$

where $\tilde{D}$ is called the "interdiffusion coefficient" because it describes a bulk intermixing process of two materials and includes the combined effects of the fluxes of all the mobile species present. Here the mobile species are Hf^{+4}, Er^{+3}, and O^{-2} ions, assuming that there are very few free electrons or holes in the system.

In the nonsteady state situation, the concentrations of the various mobile species at any position in the system are functions of time, and $\tilde{D}$ is often a function of composition. In this case Fick's First Law is difficult to apply because it requires measurement of local fluxes. Combination of Equation 4 with a continuity equation yields Fick's Second Law:

$$\frac{\partial c_i}{\partial t} = \frac{\partial}{\partial x}\left(\tilde{D}\,\frac{\partial c_i}{\partial x}\right) \qquad (5)$$

which is not so difficult to apply since local concentration changes are more easily measured than local fluxes.

Fick's Second Law with $\tilde{D}$ a function of composition (and therefore of position) is a differential equation which is not easily solved. Wagner (1969) has analyzed the interdiffusion problem in binary systems, expanding on the earlier work of Boltzmann (1894) and Matano (1933) and Sauer and Freise (1962). The Wagner approach is applicable to an experiment where the initial geometry is "doubly infinite" with a step function composition discontinuity, that is, a long diffusion couple consisting of two initially uniform halves. Wagner's approach

also allows for correction in the distance coordinate due to changes in molar volume with changes in composition and at the same time avoids the cumbersome procedure of locating a Matano interface during data analysis. The Wagner analysis allows calculation of $\tilde{D}$ from a concentration vs. distance plot according to

$$\tilde{D}(N_i^*) = \frac{(N_i^+ - N_i^-)V_m(N_i^*)}{2t(\partial N_i/\partial x)_{x=x^*}} \left[(1-Y^*)\int_{-\infty}^{x^*} \frac{Y}{V_m}\,dx + Y^*\int_{x^*}^{\infty} \frac{(1-Y)}{V_m}\,dx\right] \quad (6)$$

where N_i is the mole fraction of diffusant i

N_i^* is the mole fraction of diffusant at a particular location x^*

N_i^+ is the mole fraction of diffusant at the positive end of the interdiffusion couple, i.e. $N_i = N_i^+$ at $x = +\infty$

N_i^- is the mole fraction of diffusant at the negative end of the interdiffusion couple i.e. $N_i = N_i^-$ at $x = -\infty$

V_m is the molar volume of the solid solution

$V_m(N_i^*)$ is the molar volume of the solid solution at a particular composition N_i^*

t is the time of the interdiffusion anneal

$(\partial N_i/\partial x)_{x^*}$ is the slope of the interdiffusion profile at x^* (i.e. it is the magnitude of the concentration gradient at x^* after time t)

Y is an auxiliary variable equal to $(N_i - N_i^-)/(N_i^+ - N_i^-)$

Each of the variable terms, except V_m, are determined graphically from a plot of concentration of diffusant N_i vs. position x in a diffusion couple after an interdiffusion anneal of duration t. V_m may be calculated from experimentally-deter-

mined unit cell dimensions for the solid solutions. In this case, use was made of the data of Johnstone (1970) who measured lattice parameters at numerous HfO_2 concentrations in C-type Er_2O_3 solid solutions. Equation 7 is the least squares fit of his results:

$$a_o(N_{HfO_2}) = 10.5506 - 0.219N_{HfO_2}, \text{ Å} \qquad (7)$$

Darken (1948) considered interdiffusion in binary metallic alloys and established the relationship between the interdiffusion coefficient and the self-diffusion coefficients of the individual diffusing species. Cooper and Heasley (1966) extended Darken's analysis to interdiffusion in binary ionic systems with a common anion. Their expression for D follows:

$$\tilde{D} = \left[\frac{Z_B N_{BY} D_{s,A}(Z_Y D_{s,Y} - Z_B D_{s,B}) + Z_A N_{AY} D_{s,B}(Z_Y D_{s,Y} - Z_A D_{s,A})}{Z_A Z_Y N_{AY} D_{s,Y} - Z_A^2 N_{AY} D_{s,A} + Z_B Z_Y N_{BY} - Z_B^2 N_{BY} D_{s,B}}\right] \left(1 + \frac{d \ln \gamma_{AY}}{d \ln N_{AY}}\right) \qquad (8)$$

where Z_i is the valence of species i (i = A,B,Y)

N_i is the mole fraction of species i

$D_{s,i}$ is the self-diffusion coefficient of species i

γ_i is the activity coefficient of species i

Y is an anion species

A,B are cation species

AY,BY denote binary ionic compounds

The magnitudes of γ_i and $D_{s,i}$ vary with composition.

Self-diffusion studies of erbium and oxygen in Er_2O_3 (Berard and Wilder, 1969, and Berard et al. 1968) have shown that oxygen self-diffusion is by far faster than erbium self-diffusion. Likewise, oxygen self-diffusion in CaO-stabilized ZrO_2 has been found to be several orders of magnitude faster than the self-diffusion of either cation (Simpson and Carter, 1966, and Rhodes and Carter 1966). Noting these results and the close similarity of the crystal chemistries of Er_2O_3, stabilized ZrO_2, and stabilized HfO_2, it is reasonable to assume that oxygen self-diffusion is much faster than cation self-diffusion in the fluorite and Er_2O_3 C-type solid solution region of the Er_2O_3-HfO_2 system; that is

$$D_{s,Y} >> D_{s,A} \quad \text{and} \quad D_{s,Y} >> D_{s,B}$$

or

$$D_{s,O} >> D_{s,Hf} \quad \text{and} \quad D_{s,O} >> D_{s,Er}$$

Therefore, for this system, Equation 8 reduces to

$$\tilde{D} = \left(\frac{Z_{Er}N_{Er_2O_3}D_{s,Hf}+Z_{Hf}N_{HfO_2}D_{s,Er}}{Z_{Er}N_{Er_2O_3}+Z_{Hf}N_{HfO_2}}\right)\left(1 + \frac{d \ln \gamma_{HfO_2}}{d \ln N_{HfO_2}}\right) \qquad (9)$$

Equation 9 alone is insufficient to determine both $D_{s,Hf}$ and $D_{s,Er}$ for all experimental values of $\tilde{D}$, N_{HfO_2}, and $N_{Er_2O_3}$. However, at infinite dilution of either component, that is, at $N_{HfO_2} \approx 0$ or $N_{Er_2O_3} \approx 0$, the equation can be approximately solved for either $D_{s,Hf}$ of $D_{s,ER}$, respectively. Since this work examined $\tilde{D}$ in the Er_2O_3-rich solid solution region

exclusively, $N_{Er_2O_3} \approx 0$ did not occur experimentally, and only $D_{s,Hf}$ can be evaluated. At $N_{HfO_2} \approx 0$, Equation 9 simplifies to:

$$\tilde{D} \cong D_{s,Hf}\left(1 + \frac{d \ln \gamma_{HfO_2}}{d \ln N_{HfO_2}}\right) \qquad (10)$$

At low HfO_2 concentrations, the activity term $(d \ln \gamma_{HfO_2})/(d \ln N_{HfO_2})$ can be estimated according to the method of Whitney and Stubican (1971) which considers the formation of defects accompanying solution of aliovalent dopant at infinite dilution. Defect formation in the Er_2O_3-rich solid solutions was described in the Introduction Section and was quantified in Equation 2. It must be emphasized here that Equation 2 is at best a first approximation of the actual situation, since it disregards probable defect interactions such as the association or perhaps clustering of $Hf_{Er}^{\cdot}$ and O_i'' species, especially at higher HfO_2 concentrations.

An equilibrium constant for the reaction of Equation 2 may be written as

$$K = \frac{[Hf_{Er}^{\cdot}][O_o]^{3/2}[O_i'']^{1/2}}{a_{HfO_2}} \qquad (11)$$

where brackets represent concentration and a_{HfO_2} represents the activity of HfO_2 in the solid solution. The value of $[O_o]$ may be taken as unity, so that

$$a_{HfO_2} \cong K^{-1}[Hf_{Er}^{\cdot}][O_i'']^{1/2} \qquad (12)$$

From Equation 2, a simplified electrical neutrality condition indicates that

$$[O_i''] = \frac{1}{2}[Hf_{Er}^{\cdot}] = \frac{1}{2}N_{HfO_2} \tag{13}$$

Substitution of Equation 13 into 12 gives

$$a_{HfO_2} \cong \frac{K^{-1}}{\sqrt{2}} [Hf_{Er}^{\cdot}]^{3/2} = \frac{1}{\sqrt{2}} K^{-1} N_{HfO_2}{}^{3/2} \tag{14}$$

and

$$\gamma_{HfO_2} \equiv \frac{a_{HfO_2}}{N_{HfO_2}} \cong \frac{1}{\sqrt{2}} K^{-1} N_{HfO_2}{}^{1/2} \tag{15}$$

Therefore

$$\frac{d \ln \gamma_{HfO_2}}{d \ln N_{HfO_2}} = \frac{d \ln (\frac{1}{\sqrt{2}} K^{-1} N_{HfO_2}{}^{1/2})}{d \ln N_{HfO_2}} = \frac{1}{2} \tag{16}$$

Substitution of Equation 16 into 10 gives

$$\tilde{D}(N_{HfO_2} = 0) \approx \frac{3}{2} D_{s,Hf} \tag{17}$$

This $D_{s,Hf}$ is called the impurity diffusion coefficient of Hf in Er_2O_3 and should be nearly equal to the tracer self-diffusion coefficient for Hf at impurity levels in Er_2O_3.

At this time the author knows of no available data for Hf tracer self-diffusion in Er_2O_3. Scheidecker and Berard (1973, 1976) have used this approach to extrapolate CaF_2-SrF_2 and SrF_2-BaF_2 interdiffusion data to zero SrF_2 concentration, and have found their calculated impurity diffusion coefficients for Sr in both CaF_2 and BaF_2 in excellent agreement with previously measured tracer self-diffusion coefficients for Sr in

CaF_2 and in BaF_2 (Baker and Taylor, 1969). Likewise, Visser et al. (1975) extrapolated CaF_2-YF_3 interdiffusion data to zero YF_3 concentration and thereby estimated yttrium impurity diffusion coefficients in nearly pure CaF_2. These results indicate that the procedure described above should provide a valid estimate of Hf impurity diffusion coefficients in Er_2O_3.

PROCEDURE

Powder Preparation

Raw Er_2O_3 powder was prepared at the Ames Laboratory rare earths pilot plant by precipitation and calcination of erbium oxalate. Analysis by mass spectroscopy indicated that the summed concentration of all impurities was less than 60 ppm, 30 ppm of which were Cl^-. This as-received powder proved unsuitable for sintering to the 95%-99% theoretical density which is characteristic of the continuous and unobstructed microstructure suitable for bulk diffusion studies. A sinterable Er_2O_3 powder was produced by dissolving the as-received oxide followed by precipitation and calcination of $Er(OH)_3$.

Addition of 55 ml of concentrated HNO_3 was made to a hot, stirred mixture of 50 grams as-received Er_2O_3 in 50 ml water. The mixture was heated and stirred in a covered glass beaker until the oxide had dissolved. The solution was cooled to room temperature, filtered, and diluted with water to 500 ml. Assuming total solution of the oxide, the concentration of the solution was 100 grams Er_2O_3 per liter or 0.262 M Er_2O_3.

The solution was dripped at the approximate rate of 10 ml per minute into a vigorously stirred solution of 100 ml concentrated NH_4OH in 100 ml water. A gelatinous precipitate was formed which was separated from the solution by centrifuging. The centrifuged precipitate, about 300 ml in volume, was broken up for washing and was added to roughly 4 liters

of water. An addition of 150 ml concentrated NH_4OH was used to make a washing solution which would prevent dispersion and peptization of the precipitate. The mixture was stirred vigorously for 1 hour, then left standing in order to settle the precipitate. The supernatant liquid was decanted and the precipitate was centrifuged.

The caked precipitate was placed on filter paper inside a glass beaker. The beaker was covered with a watchglass and held at 100°C in a vented laboratory drying oven for 16 hours. The covered beaker arrangement was necessary in order to slow the drying rate of the hydroxide sufficiently to enhance the sinterability of the oxide powder. The importance of the drying rate has been noted by Visser, Schiavi, and Berard (1976) in a concurrent study.

The dried hydroxide was crushed to -200 mesh using an agate mortar and pestle. The powder was placed in an open platinum dish and calcined in air for 3 hours at 600°C in an electric resistance heated muffle furnace. A prior thermogravimetric analysis had indicated that the 600°C calcine was adequate for complete conversion to Er_2O_3.

HfO_2-doped Er_2O_3, henceforth abbreviated HDE, was prepared by a procedure analogous to the preparation of undoped Er_2O_3. An intimate mixture of gelatinous $Er(OH)_3$ and $Hf(OH)_4$ was coprecipitated from a volumetrically prepared mixture of two solutions. The HfO_2 solution was an aqueous solution of

hafnium oxychloride ($HfOCl_2 \cdot 8H_2O$). The concentration was 94.32 grams HfO_2 per liter or 0.448 M HfO_2. The commercially prepared $HfOCl_2 \cdot 8H_2O$ was analyzed for cation impurities by emission spectroscopy. The results are listed in Table 1. The Er_2O_3 solution was prepared by the same procedure as the Er_2O_3-HNO_3 solution except that HCl was used instead of HNO_3. The concentration of the Er_2O_3 solution was equal to 100 grams Er_2O_3 per liter or 0.262 M Er_2O_3.

Table 1. Emission spectrographic analysis of hafnium oxychloride

Element	Concentration ppm	Element	Concentration ppm
Al	<25	Mo	<10
B	<0.2	Ni	<10
Cb	<100	Pd	<5
Cd	<1	Si	<40
Co	<5	Sn	<10
Cr	<10	Ta	<200
Cu	<40	Ti	<20
Fe	<50	V	<5
Mg	<10	W	<20
Mn	<10	Zr	64

A mixture consisting of 38.5 ml of the HfO_2 solution and 240.2 ml of the Er_2O_3 solution was prepared. The mixture was diluted to 300 ml in order to establish the concentration at 100 grams total oxide per liter solution, which was equal to the concentration of the undoped Er_2O_3 solution. The mixed solution was stirred approximately 1 hour and then dripped into a solution of 60 ml concentrated NH_4OH and 60 ml water.

The hydroxide precipitate was washed repeatedly with very dilute NH_4OH until nearly all the dissolved NH_4Cl was removed. The presence of the chloride ion in the supernate was tested by the addition of dilute $AgNO_3$ solution. This washing procedure was undertaken because residual chloride in the precipitate would chemically combine with the hydroxides during calcining and remain present throughout sintering. On the other hand, the NH_4NO_3 salts in the undoped $Er(OH)_3$ precipitate decomposed and escaped during calcining, and thorough washing was not necessary.

The washed mixed hydroxide was dried, crushed, and calcined in the same manner as in the previously described preparation of undoped Er_2O_3. The molar ratio of HfO_2 to Er_2O_3 was determined by wet chemical analysis of the dried hydroxide, and translated into 19.51 mole % HfO_2 in the calcined product.

Pellet Preparation

The calcined oxide powders, both HDE and undoped Er_2O_3, were pressed into pellets at 11,000 psi in a 3/8-inch diameter double acting steel die, and repressed isostatically at 30,000 psi. The pressed pellets each weighed approximately 1 gram and were about 1/4-inch thick. The pellets were stacked for sintering inside a covered 1-inch diameter Er_2O_3 crucible. Fine gauge tungsten wires were used for separators.

The pellets were vacuum sintered at 2000°C for 3 hours. The vacuum was held below 2×10^{-5} torr except during heat-up

when some outgassing occurred. Both the heating and cooling rates for the HDE sintering were 50°C per minute. The heating rate for the undoped Er_2O_3 was slowed to 10°C per minute in order to decrease the tendency for exaggerated grain growth in the early stages of sintering and in so doing to allow more time for the elimination of pores along grain boundaries. The cooling rate for the undoped Er_2O_3 was 50°C per minute. In the sintering of HDE, the HfO_2 dopant retarded the rate of grain growth to the extent that a lower heating rate was not deemed necessary.

The sintering furnace[1] consisted of a water-cooled stainless steel vacuum chamber enclosing a cylindrical tungsten mesh resistance heating element. The Er_2O_3 crucible was supported in the work zone on a tungsten-capped tantalum pedestal. Tantalum and molybdenum radiation shields surrounded the heating element and the work zone and protected the stainless steel enclosure. Crucible temperature was measured with an optical pyrometer[2]. A molybdenum sheathed W 5% Re-W 26% Re thermocouple protruded into the work zone to within 1 inch of the Er_2O_3 crucible. An automatic control system monitored the thermocouple output and maintained the furnace temperature within $\pm$ 5°C around the sintering temperature.

---

[1]Model 15, Centorr Associates, Suncook, NH.

[2]Model 8622-C, Leeds and Northrup Co., Philadelphia, PA.

During vacuum sintering, both the Er_2O_3 and HDE pellets were slightly reduced. To reoxidize the pellets, they were heated in air to 1200°C and held at temperature for 2 hours. All of the reoxidized pellets were quite translucent; several of the reoxidized HDE pellets were transparent.

The densities of the reoxidized pellets were measured by water immersion. The sintered densities of the Er_2O_3 pellets ranged from 97.0% to 98.0% of theoretical density; the densities of the HDE pellets ranged from 97.0% to 99.0% theoretical density. The theoretical densities of undoped Er_2O_3 and of HDE, calculated from the lattice parameter data of Johnstone (1970), are respectively 8.65 grams/cm^3 and 8.87 grams/cm^3.

The microstructure of the sintered oxides were examined. Figures 2 and 3 are reflected light photomicrographs of the sintered pellets etched to reveal the grain boundaries. The undoped Er_2O_3 grains were approximately 20 μm in diameter and contained numerous pores. The average diameter of the HDE grains was 3 μm and the microstructure was almost pore-free.

The pellets were mounted, one face exposed, in low melting wax[1] inside stainless steel rings approximately 1 inch in diameter. The exposed faces were lapped flat with 5 μm alumina in oil on a slotted cast iron lap plate[2]. The flat surfaces were polished with 0.3 μm alumina in oil on a cloth-

[1]Rigidax, Type W1-Green, M. Argueso and Co., Inc., Mamaroneck, NY.

[2]Lapmaster Model 12, Crane Packing Co., Morton Grove, IL.

Figure 2. Photomicrograph of sintered undoped Er_2O_3. 81X

Figure 3. Photomicrograph of sintered HDE. 403X

covered lapping plate[1]. Each pellet was lapped and polished until it was optically flat as checked with an interferometer-type flatness tester[2] using thallium light (λ = 0.535 μm). The wax was melted away and each lapped pellet was thoroughly cleaned using methanol.

Diffusion Experiments

The polished faces of an Er_2O_3 pellet and a HDE pellet were mated to form a diffusion couple. Each couple was tied together with graphite thread to prevent shifting during handling. For the diffusion anneals, three couples were placed with the Er_2O_3 on the bottom of an Er_2O_3 crucible which was covered but also vented to maintain air circulation around the couples.

Diffusion anneals were conducted inside the work chambers of natural gas-fired tube furnaces. The tubes were vented to the atmosphere to allow air circulation. The anneal temperatures and respective times are listed in Table 2. No corrections for heating and cooling times were required because of the long anneal times.

The 1900°C, 1850°C, and 1800°C anneals were conducted in a stabilized-zirconia-lined furnace[3] heated by a natural gas-oxygen-air mixture. The diffusion couple temperature was

---

[1]Texmet Cloth, Buehler, Ltd., Evanston, IL.

[2]Model 64-31-01, Carl Zeiss, West Germany.

[3]Model LOF-3, Lemont Scientific, Inc., Lemont, PA.

Table 2. Diffusion anneals

Temperature, °C	Time, hours
1900	14
1850	18
1800	28
1700	60
1600	182

determined with an optical pyrometer[1]. Furnace temperature was held within ± 10°C by an automatic system which compared a preset millivoltage to the output of a Pt 6% Rh-Pt 30% Rh thermocouple. The thermocouple was located inside the tube of the furnace, but removed from the Er_2O_3 crucible to a cooler zone within the useful range of the thermocouple, that is, not higher than 1700°C.

The 1700°C and 1600°C anneals were conducted in an alumina-lined natural gas-air furnace[2]. The furnace temperature was monitored and controlled according to the output of a Pt 6% Rh-Pt 30% Rh thermocouple with the sensing junction within 1/2-inch of the Er_2O_3 crucible.

The annealed couples were mounted in room temperature setting acrylic[3] and cut parallel to the diffusion direction. The exposed surface was ground and polished with 0.3 μm alumina and water, and a carbon coating was applied by vacuum

[1]Model 8622-C, Leeds and Northrup Co., Philadelphia, PA.

[2]Model 2150, Bickley Furnaces, Inc., Philadelphia, PA.

[3]Flash Acrylic, Yates Manufacturing Co., Chicago, IL.

evaporation. Figure 4 is a reflected light photomicrograph of the ground and polished 1850°C couple with no carbon coating. The microstructures of the undoped Er_2O_3 and the HDE are clearly distinguishable, as are the remnant of the couple interface and the diffusion zone.

HfO_2 and Er_2O_3 concentration profiles were determined by simultaneous counting of Hf M_α and Er L_α x-rays using an electron microprobe[1]. The 15 KV, 0.015 μA beam was focused to a 1 μm diameter spot which was usually oscillated at 100 Hz over a 75 μm distance perpendicular to the diffusion direction and was manually step-scanned parallel to the diffusion direction. X-ray intensities were corrected for absorption and other errors and converted to mole percents HfO_2 and Er_2O_3 using the MAGIC Version IV computer program[2]. The composition mapping procedure was repeated at two different diametral locations in each diffusion couple.

---

[1]Model XMA-S, Hitachi, Ltd., Tokyo, Japan.

[2]Available from J. W. Colby, Bell Telephone Laboratories, Inc., Allentown, PA.

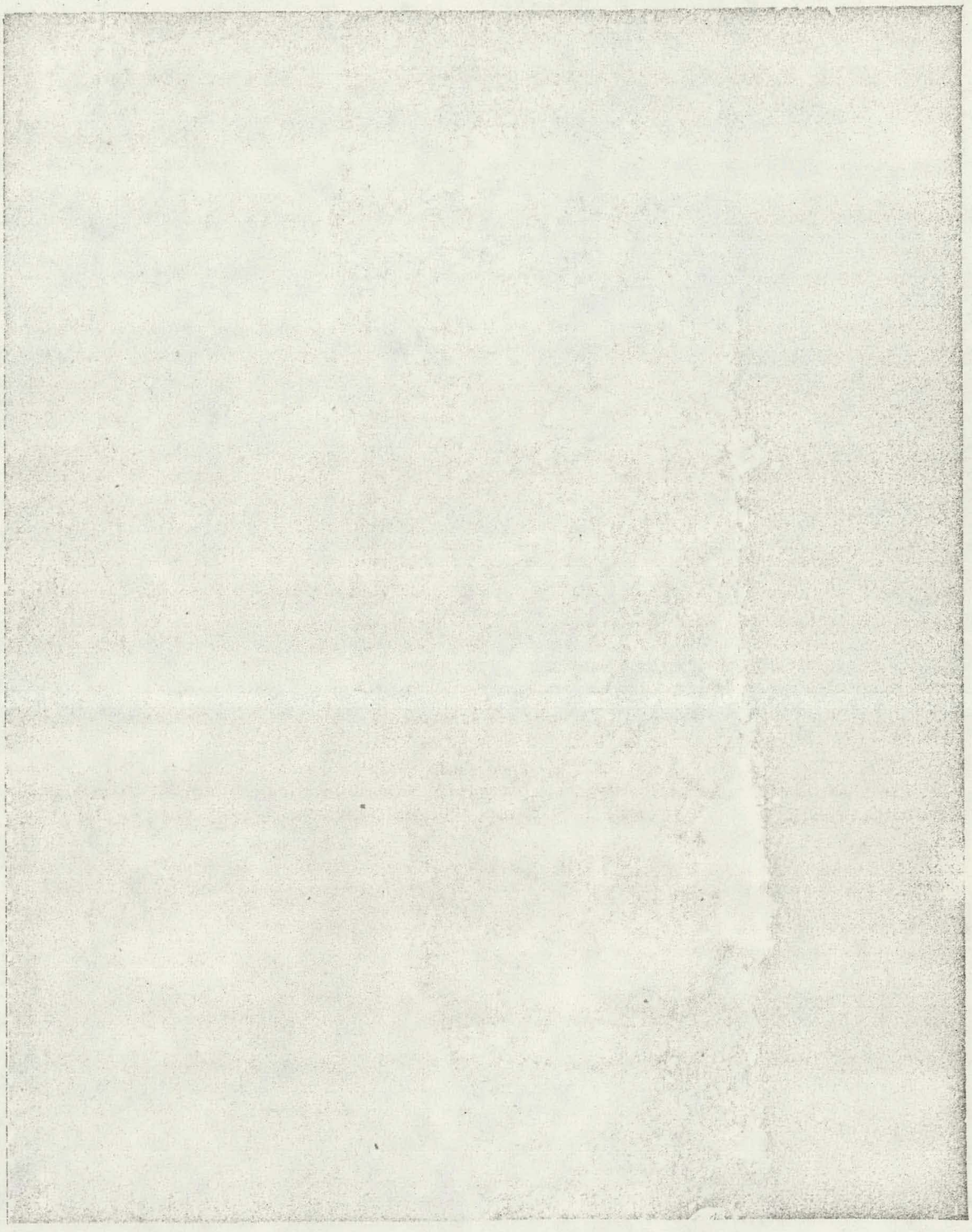

Figure 4. Photomicrograph of 1850°C diffusion couple interface and diffusion zone. HDE on left. Er_2O_3 on right. 81X

RESULTS AND DISCUSSION

All interdiffusion composition profiles are compiled in the Appendix in Figures A1 through A11. A scaled plot was generated from each profile by dividing the compositions at each position $N^*_{HfO_2}$ on the raw profile by the appropriate $V_m(N^*_{HfO_2})$. Experimental values of the interdiffusion coefficient at selected $N^*_{HfO_2}$ values were then calculated using Equation 18, a rearrangement of Equation 6.

$$\tilde{D}(N^*_{HfO_2}) = \frac{V_m(N^*_{HfO_2})}{2t(\partial N_{HfO_2}/\partial x)_{x=x^*}} [(1-Y^*)\int A + Y^* \int B] \qquad (18)$$

Figure 5 is a schematic of a raw and scaled composition profile illustrating the graphical determination of the variable terms in Equation 18. The slope $(\partial N_{HfO_2}/\partial x)_{x=x^*}$ was measured directly from the raw penetration profile. The areas $\int A$ and $\int B$ were measured from the scaled profile using a polar planimeter[1]. The calculated $\tilde{D}$ values are listed in Tables A1 through A5 in the Appendix.

The interdiffusion coefficients are shown as a function of composition and temperature in Figures 6 and 7. Each data point represents the average of the two measurements made at different diametral locations in the same interdiffusion couple. Only one set of $\tilde{D}$ values was computed for the 1600°C anneal because the second diametral location was cracked in

---

[1]Model 22084, Crosby Steam Gauge and Valve Co., Boston, MA.

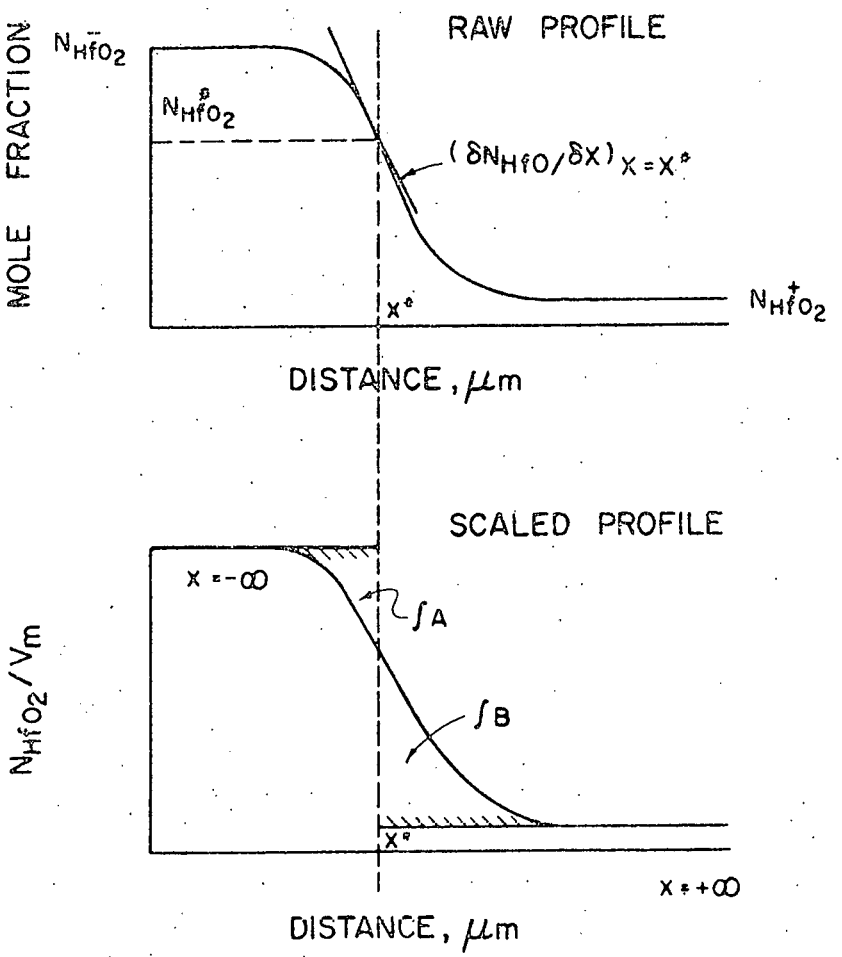

Figure 5. Schematic sketch of raw experimental data and scaled experimental data for calculating interdiffusion coefficients

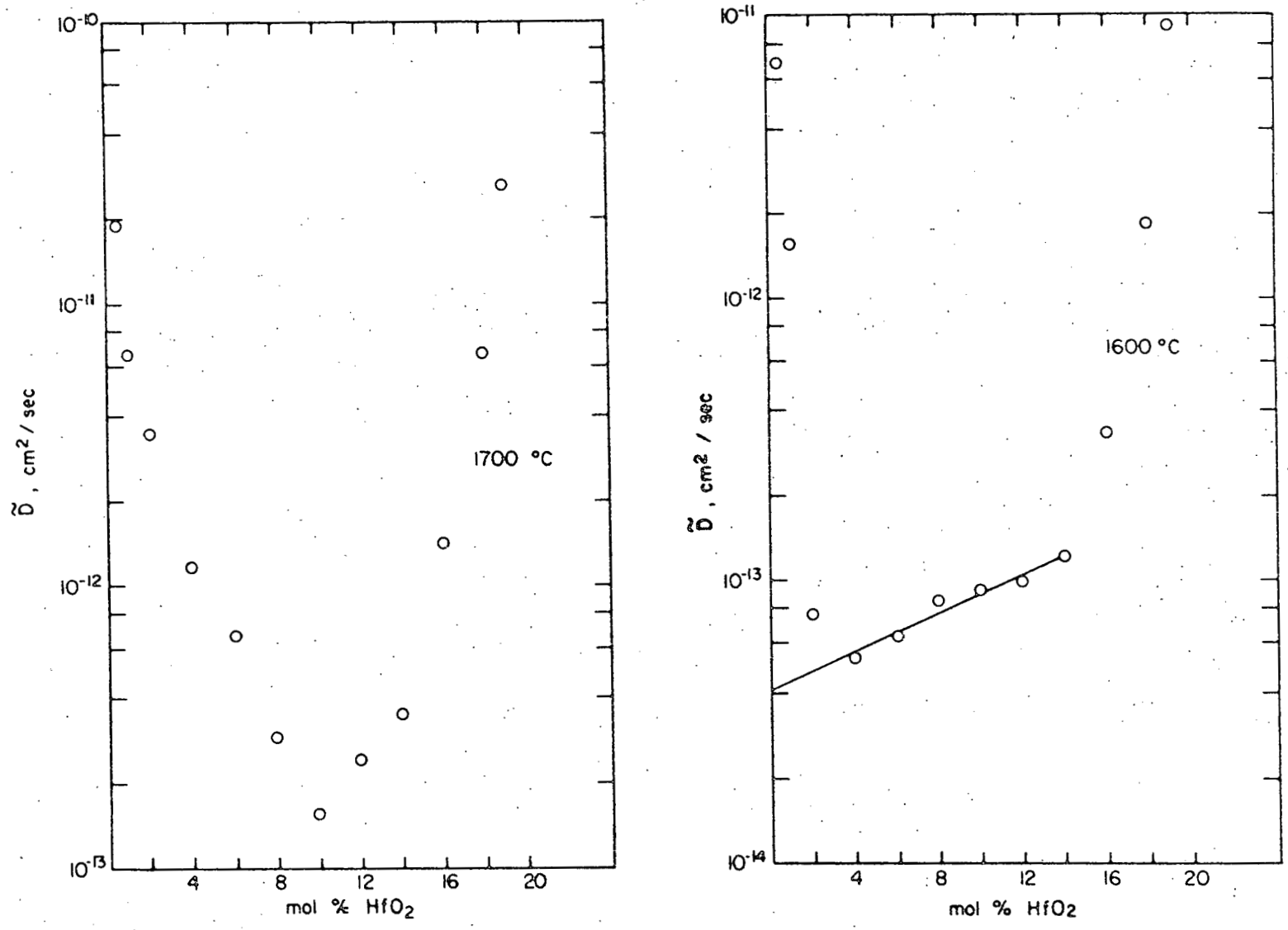

Figure 6. Interdiffusion coefficients in Er_2O_3-HfO_2 solid solutions

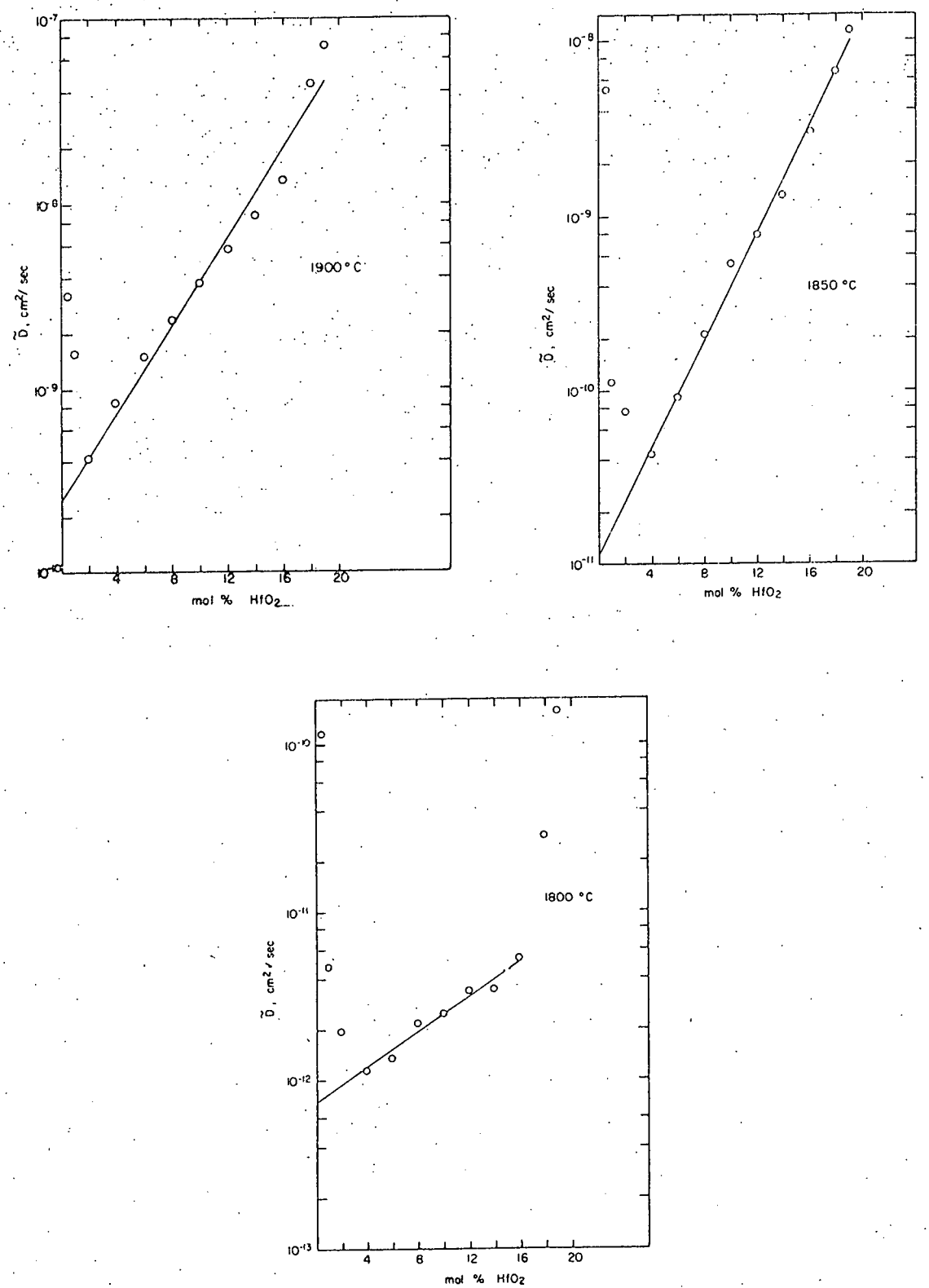

Figure 7. Interdiffusion coefficients in Er_2O_3-HfO_2 solid solutions

the diffusion zone, and the profile obtained was inadequate for calculation of $\tilde{D}$. The composition dependences of $\tilde{D}$ at each temperature except 1700°C are characterized by a minimum in the range 2-4 mole % HfO_2 followed by a continuous increase in $\tilde{D}$ with increasing N_{HfO_2}.

In the Introduction it was proposed that the predominating intrinsic defects in pure Er_2O_3 are anion Frenkel pairs. The solution of HfO_2 into Er_2O_3, described in Equation 2, causes the formation of oxygen interstitials. Thus, doping Er_2O_3 with HfO_2 will increase the concentration of oxygen interstitials, which will reduce the concentration of oxygen vacancies through the anion Frenkel equilibrium. This reduction of oxygen vacancy concentration will promote an increase in the erbium vacancy concentration through the Schottky equilibrium. If the cations migrate by a vacancy jump mechanism, then cation mobilities can be expected to increase with HfO_2 concentration. This explanation is consistent with the observed increase in experimental $\tilde{D}$ with N_{HfO_2}, but it is oversimplified in excluding the effects of probable defect interactions at high dopant levels. The Cooper-Heasley relation, Equation 9, also predicts that if $D_{s,Er} > D_{s,Hf}$, $\tilde{D}$ will increase with N_{HfO_2}. This is thus an indirect indication the $D_{s,Er}$ is indeed greater than $D_{s,Hf}$. This prediction does not account for probable changes in the magnitude of the activity term $(d \ln \gamma_{HfO_2})/(d \ln N_{HfO_2})$ and again the possible effects of defect interactions have been disregarded.

The data for all temperatures except 1700°C can be reasonably well represented over the range 2-18 mole % HfO_2 by an equation of the form

$$\tilde{D} = \tilde{D}' \exp(b\, N_{HfO_2}) \qquad (19)$$

where $\tilde{D}'$ and b are curve fitting constants. The data at 1700°C, however, reach a minimum at 10 mole % HfO_2. This behavior is anomalous as compared to that at the other four temperatures and therefore the 1700°C data has not been included in subsequent analyses.

Least squares fits to Equation 19 are shown in Figures 6 and 7 and the values of $\tilde{D}'$ and b are given in Table 3. The values of b increase generally with increasing temperature indicating an increase in the composition dependence of D as higher temperatures are reached. This same exponential form for the composition dependence of $\tilde{D}$ was reported by Visser et al. (1975) in the YF_3-CaF_2 system, but the values of b were there found to decrease with increasing temperature.

The magnitude of the constant $\tilde{D}$ in Equation 19 can be interpreted to represent the value of $\tilde{D}(N_{HfO_2}=0)$ if it is assumed that the exponential composition dependence of $\tilde{D}$ actually extends down to 0 mole % HfO_2. Using the arguments developed in Equations 7-17 suggests that multiplying the values of $\tilde{D}'$ by 2/3 would then yield estimates of $D_{s,Hf}$, the impurity diffusion coefficient of Hf in pure Er_2O_3. These estimates are also given in Table 3. A least squares fit of

Table 3. Empirical coefficients for $\tilde{D} = \tilde{D}' \exp(b\, N_{HfO_2})$

Temperature, °C	Linear range, mol %	$\tilde{D}'$, cm^2/sec	b	$D_{s,Hf}$, cm^2/sec[a]
1900	2-19	2.46×10^{-10}	27.6	1.64×10^{-10}
1850	4-19	1.14×10^{-11}	35.5	7.60×10^{-12}
1800	6-16	7.39×10^{-13}	11.9	4.93×10^{-13}
1600	4-14	4.00×10^{-14}	8.0	2.67×10^{-14}

[a]Evaluated as (2/3 $\tilde{D}'$); see Equation 17.

Table 4. Empirical coefficients for $\tilde{D}(N_{HfO_2} \approx 0)$ and $D_{s,Hf}$ Evaluated from 4%-2% extrapolations

Temperature, °C	$\tilde{D}(N_{HfO_2} \approx 0)$, cm^2/sec	$D_{s,Hf}$, cm^2/sec[a]
1900	2.03×10^{-10}	1.53×10^{-10}
1850	1.34×10^{-10}	8.93×10^{-11}
1800	3.22×10^{-12}	2.15×10^{-12}
1600	1.10×10^{-13}	7.33×10^{-14}

[a]Evaluated as [2/3 $\tilde{D}(N_{HfO_2} \approx 0)$]; see Equation 17.

these estimated impurity diffusion coefficient values to the Arrhenius equation yields

$$D_{s,Hf} = (3.28\ ^{+8.53}_{-2.37})\times 10^{10}\exp\left(\frac{-209\pm 45\ \text{Kcal/mole}}{RT}\right)\text{cm}^2/\text{sec} \qquad (20)$$

The above extrapolation from a heavily-doped extrinsic region (2-18% HfO_2) down to a presumably intrinsic region (~0% HfO_2) is at best a rough approximation. In addition, the validity of this simple extrapolation is certainly questionable since $\tilde{D}$ shows a definite upturn in the region below 4% HfO_2. The uncertainty in $\tilde{D}$ at low HfO_2 contents is large, however, since the graphical determination of $\tilde{D}$ from a composition profile is inherently unaccurate at the tails of the profile, and the upturn of $\tilde{D}$ may well be an artifact. In this particular experiment, the data points are noticeably scattered at the tails of the profiles. As an alternative way of approximating $\tilde{D}(N_{HfO_2}\approx 0)$, the line passing through the $\tilde{D}$ values at 2% and 4% HfO_2 was extrapolated to 0% HfO_2. The values of $\tilde{D}(N_{HfO_2}=0)$ and $D_{s,Hf}$ estimated in this way are listed in Table 4. A least squares fit of these values to the Arrhenius equation yields

$$D_{s,Hf} = (3.63^{+5.81}_{-2.23})\times 10^{10}\exp\left(\frac{-204\pm 34\ \text{Kcal/mole}}{RT}\right)\text{cm}^2/\text{sec} \qquad (21)$$

Whether either Equation 20 or 21 approximate the correct values of $D_{s,Hf}$ in pure Er_2O_3 will remain a matter of speculation until accurate tracer measurements of Hf impurity diffu-

sion coefficients in Er_2O_3 are accomplished.

The temperature dependence of $\tilde{D}$ is shown as a function of composition in Figures 8 through 10, and the Arrhenius constants for these lines are given in Table 5. The least-squares fits to the Arrhenius equation do not include the values of $\tilde{D}$ at 1700°C because of the aforementioned anomalous behavior of the composition dependence of $\tilde{D}$ at this temperature. The data points at compositions of 19%, 1% and 0.5% HfO_2 are excluded from these fits because of the uncertainties in calculating $\tilde{D}$ at the tails of the profiles. The activation energies, Q, for interdiffusion increase with N_{HfO_2} to a maximum at 12% HfO_2. This is shown graphically in Figure 11.

The activation energies for interdiffusion in the heavily-doped Er_2O_3 matrix are very large compared to a reported value of 102 Kcal/mole for erbium self-diffusion in pure Er_2O_3 (Berard and Wilder, 1969). Furthermore, the standard deviations of the Q values are quite large. The standard deviation on Q can be dramatically reduced by using data only at 1900°, 1850°, and 1600°C, but the magnitude of Q still remains very large (see Table 6).

The large magnitudes of Q suggest that the mechanism of interdiffusion is not simply a straightforward cation vacancy jump process. Clearly the possibility of the interaction of charged defects must be considered. It is possible that the vacancy jumping process is hindered by the anchoring of

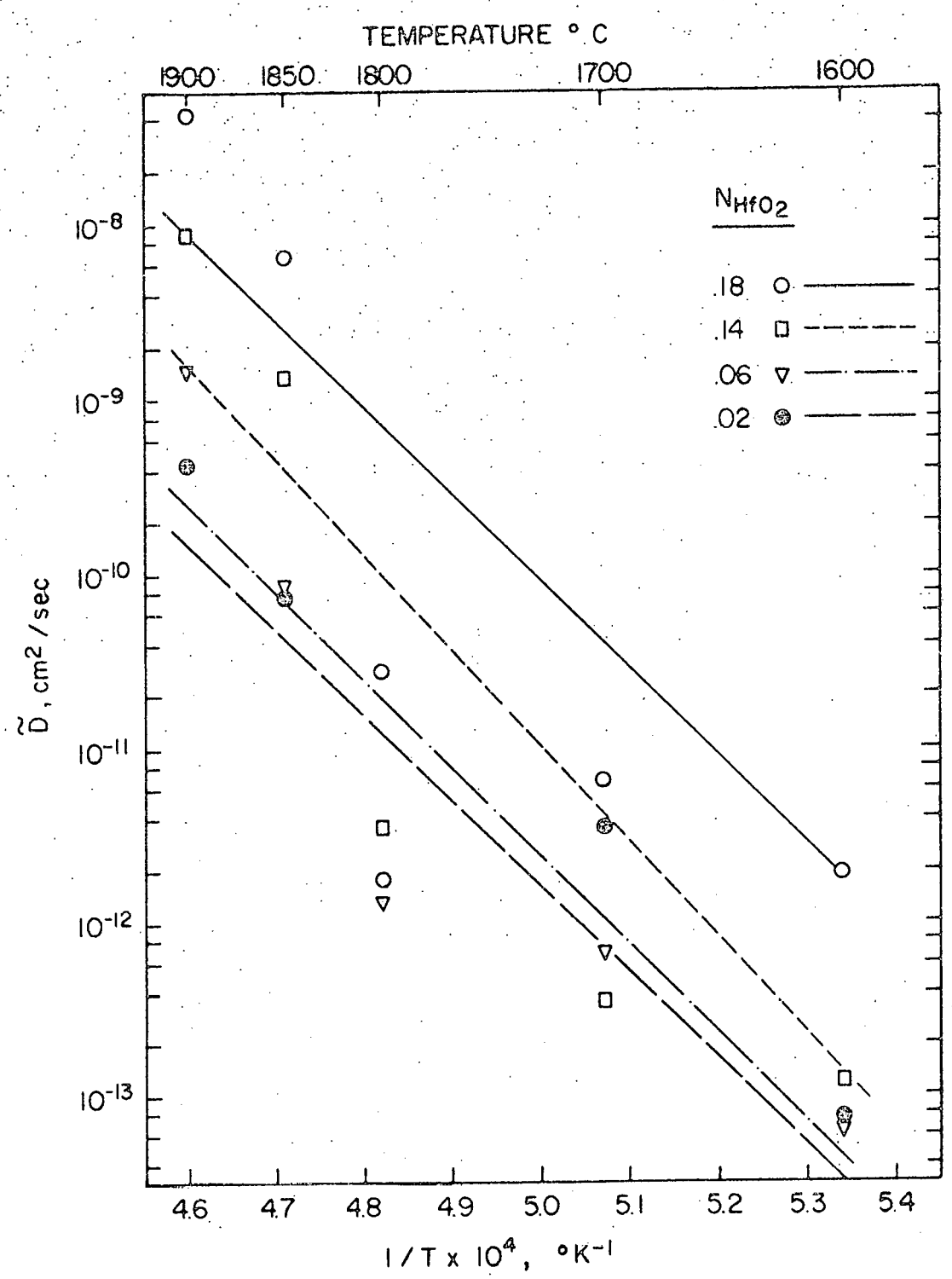

Figure 8. Temperature dependence of interdiffusion coefficients in Er_2O_3-HfO_2 solid solutions

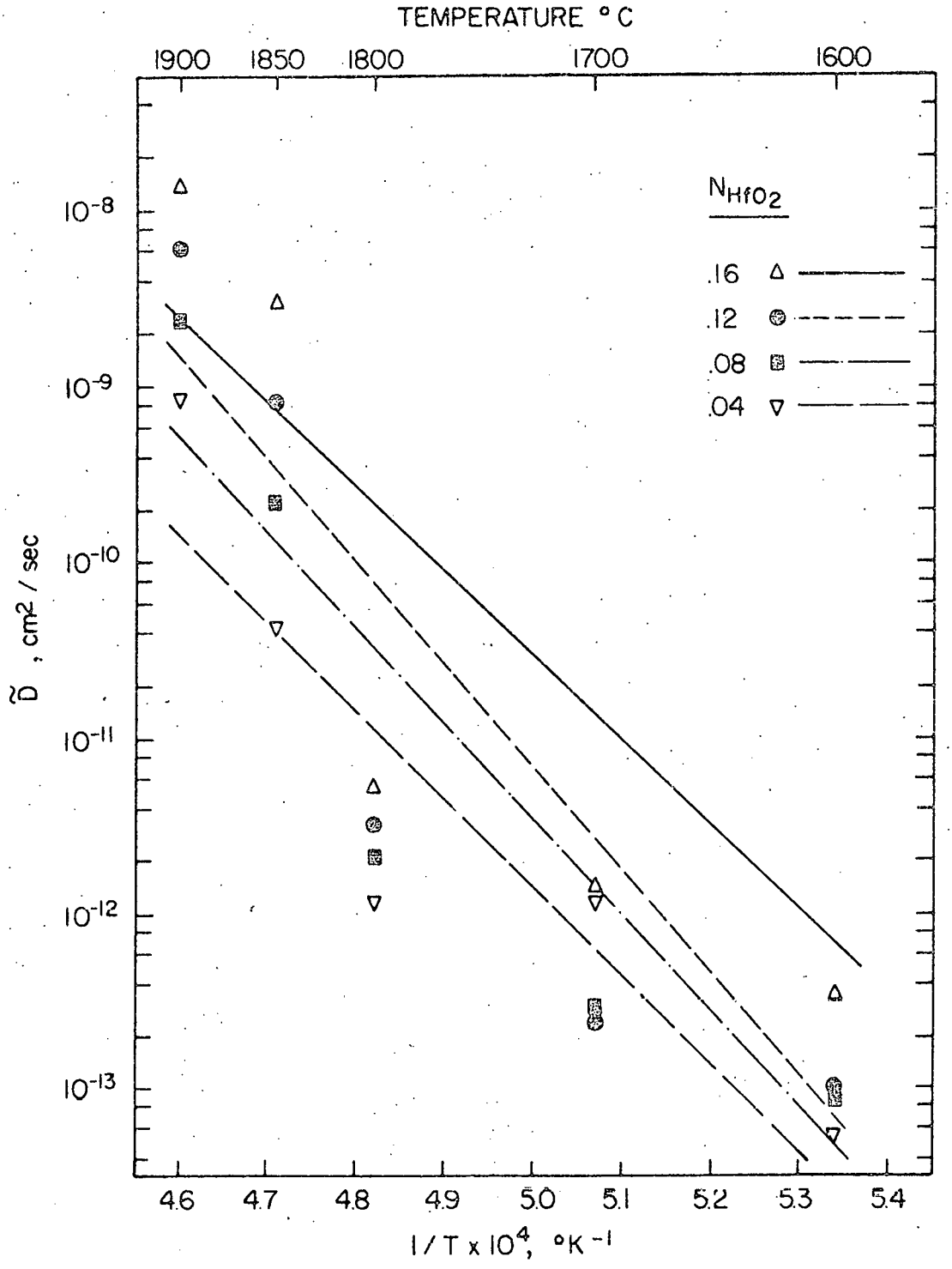

Figure 9. Temperature dependence of interdiffusion coefficients in Er_2O_3-HfO_2 solid solutions

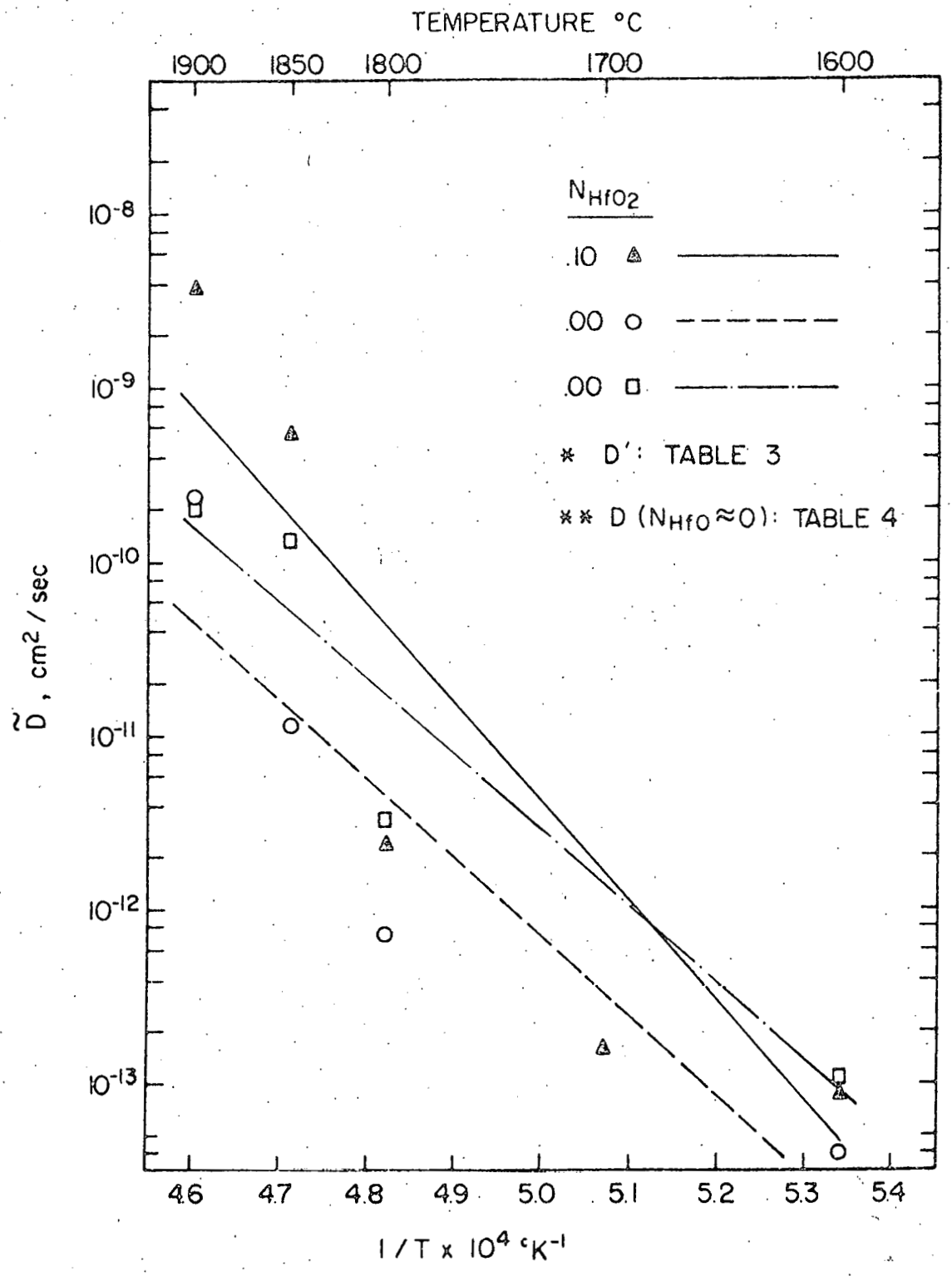

Figure 10. Temperature dependence of interdiffusion coefficients in Er_2O_3-HfO_2 solid solutions

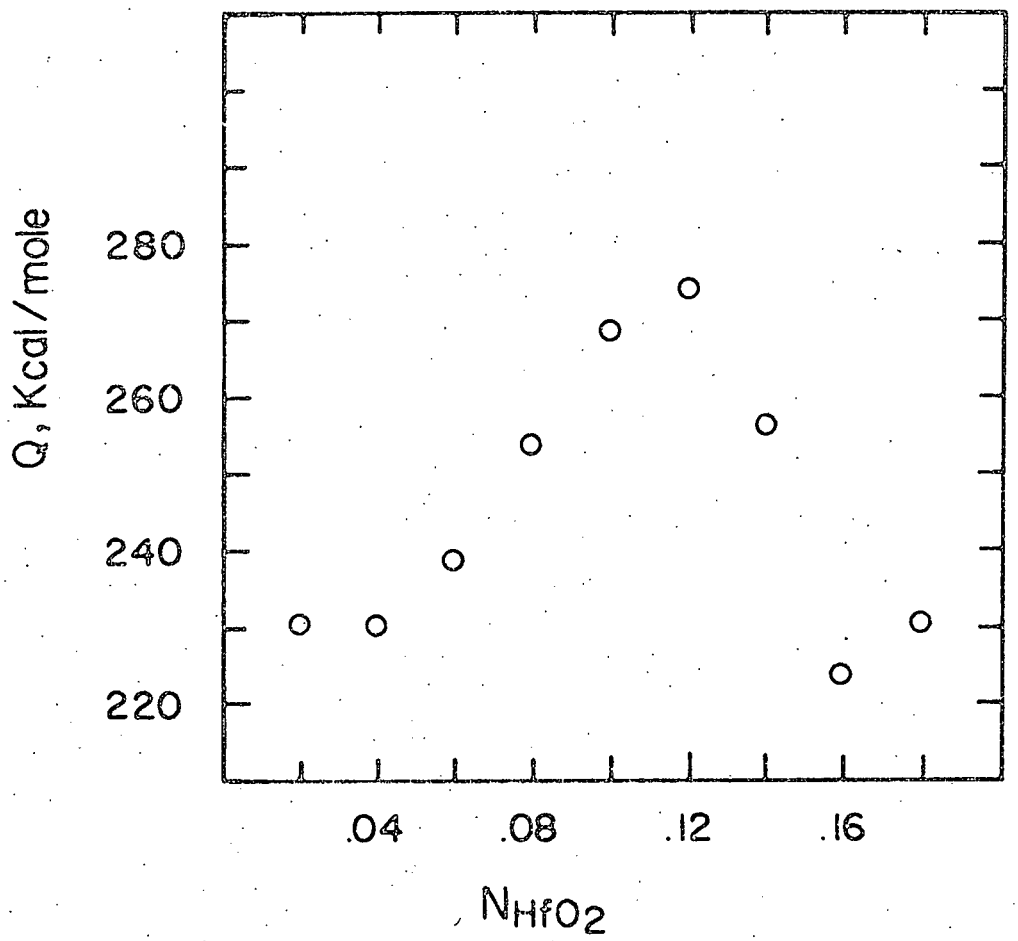

Figure 11. Composition dependence of interdiffusion activation energy

Table 5. Arrhenius constants for $\tilde{D}$ as a function of composition

N_{HfO_2}	$\tilde{D}_o$, cm^2/sec	Q, Kcal/mole
.18	$1.59^{+8.97}_{-1.35} \times 10^{15}$	231 ± 67
.16	$8.69^{+69.9}_{-7.73} \times 10^{13}$	224 ± 77
.14	$1.25^{+8.02}_{-1.08} \times 10^{17}$	257 ± 71
.12	$5.92^{+28.5}_{-4.90} \times 10^{18}$	274 ± 62
.10	$1.02^{+4.78}_{-8.38} \times 10^{18}$	269 ± 61
.08	$1.91^{+7.43}_{-1.16} \times 10^{16}$	254 ± 56
.06	$3.12^{+12.5}_{-2.50} \times 10^{14}$	239 ± 57
.04	$2.48^{+8.41}_{-1.92} \times 10^{13}$	231 ± 52
.02	$2.74^{+5.51}_{-1.83} \times 10^{13}$	231 ± 39
.00[a]	$4.92^{+12.8}_{-3.55} \times 10^{10}$	209 ± 45
.00[b]	$5.45^{+8.71}_{-3.35} \times 10^{10}$	204 ± 34

[a] Evaluated from $\tilde{D}'$ values in Table 3.

[b] Evaluated from $\tilde{D}(N_{HfO_2} \approx 0)$ in Table 4.

Table 6. Arrhenius constants of $\tilde{D}$ as a function of composition, excluding 1800°C values of D

$NHfO_2$	$\tilde{D}_o$, cm^2/sec	Q, Kcal/mole
.18	$9.37^{+2.48}_{-1.96} \times 10^{16}$	243 ± 8
.16	$1.02^{+.09}_{-.08} \times 10^{16}$	238 ± 3
.14	$9.51^{+1.67}_{-1.42} \times 10^{18}$	269 ± 6
.12	$2.63^{+.50}_{-.42} \times 10^{20}$	286 ± 6
.10	$4.36^{+.79}_{-.67} \times 10^{19}$	280 ± 6
.08	$5.47^{+2.72}_{-1.82} \times 10^{17}$	264 ± 14
.06	$8.54^{+6.86}_{-3.81} \times 10^{15}$	249 ± 21
.04	$4.66^{+4.60}_{-2.32} \times 10^{14}$	239 ± 24
.02	$2.92^{+.52}_{-.44} \times 10^{14}$	238 ± 6
.00[a]	$3.99^{+1.40}_{-1.04} \times 10^{11}$	210 ± 11

[a]Evaluated from $\tilde{D}'$ values in Table 8.

negatively charged Er vacancies (V_{Er}''') in the vicinity of reasonably immobile substitutional Hf ions ($Hf_{Er}^{\cdot}$). Above some possibly very low threshold N_{HfO_2}, a large fraction of the available Er vacancies may become thus pinned, and a high dissociation energy would then be required to free the vacancies to take part in the diffusion process. The effect of vacancy pinning should diminish at very low levels of N_{HfO_2}, and Q should decrease substantially since a large proportion of the available V_{Er}''' should then be free to provide for cation diffusion. This expected large decrease in Q is not found in the data, but the threshold N_{HfO_2} for significant vacancy pinning may well be far below the level at which accurate values of $\tilde{D}$ can be determined by graphical analysis.

A second possibility is a strong association or clustering of positive $Hf_{Er}^{\cdot}$ and negative O_i'' species. If this is the situation, then two modes of Hf diffusion are feasible, both probably requiring high Q. The $Hf_{Er}^{\cdot}$ and O_i'' species might move independently of one another and a dissociation energy would be required to break apart the complexes. Alternatively, the $Hf_{Er}^{\cdot}$ and O_i'' complex might diffuse as a unit. In this instance the movement of the large complex would introduce local strain in the lattice and the energy of motion would be increased accordingly. These two schemes of $Hf_{Er}^{\cdot}$ and O_i'' clustering are consistent with the relatively large Q at all dopant levels including very low N_{HfO_2} since every $Hf_{Er}^{\cdot}$ should be associated

with an O_i''.

Both proposed mechanisms of defect interaction, $Hf_{Er}^{\cdot}+V_{Er}^{'''}$ and $Hf_{Er}^{\cdot}+O_i''$, are insufficient to explain a peak in Q at 12% HfO_2. The nonlinear character of the temperature dependence of $\tilde{D}$ shown in Figures 8 through 10 suggests that the magnitude of Q at high temperatures might be greater than the values shown in Table 5. The overall picture is thus certainly more involved than the simple defect models proposed here. It is even possible that there exists a balance of complicated defect mechanisms which continuously changes with temperature. A comprehensive description of cation diffusion in Er_2O_3-HfO_2 solid solutions will require measurement of both cation self-diffusion coefficients and a detailed examination of defects and their interactions.

CONCLUSIONS

1. The interdiffusion coefficient shows an approximately exponential composition dependence over the range 2-18 mole % HfO_2 in Er_2O_3. This composition dependence increases as temperature increases.

2. Extrapolation of interdiffusion coefficient data to $N_{HfO_2} = 0$ allows rough estimation of the impurity diffusion coefficients for Hf in essentially pure Er_2O_3. These coefficients are lower in magnitude and higher in temperature dependence than published Er self-diffusion coefficients in undoped Er_2O_3.

3. The temperature dependence of the interdiffusion coefficient increases with HfO_2 concentration in the range 2-12 mole % HfO_2, and decreases in the range 12-18 mole % HfO_2.

BIBLIOGRAPHY

Baker, M., and Taylor, A. 1969. Cation diffusion in fluorite single crystals. J. Phys. Chem. Solids 30(4):1003-1007.

Basler, D. B., and Berard, M. F. 1974. Oxygen diffusion measurements in Dy_2O_3 and Gd_2O_3 from elevated temperature studies of the oxidation of metals. J. Amer. Ceram. Soc. 57(10):447-449.

Berard, M. F. 1971. Self-diffusion of Ca in single-crystal CaF_2. J. Amer. Ceram. Soc. 54(3):144-146.

Berard, M. F., and Wilder, D. R. 1969. Cation self-diffusion in polycrystalline Y_2O_3 and Er_2O_3. J. Amer. Ceram. Soc. 52(2):85-88.

Berard, M. F., Wirkus, C. D., and Wilder, D. R. 1968. Diffusion of oxygen in selected monocrystalline rare earth oxides. J. Amer. Ceram. Soc. 51(11):643-647.

Boltzmann, L. 1894. Ann. Phys. 53:959.

Buckley, J. D. 1969. Deterioration of calcia-stabilized zirconia. NASA TN (Technical Note) D-1595. National Aeronautics and Space Administration, Washington, D.C.

Buckley, J. D., and Wilder, D. R. 1969. Effects of cyclic heating and thermal shock on hafnia stabilized with calcia, magnesia, and yttria. NASA TN D-5279. National Aeronautics and Space Administration, Washington, D.C.

Cooper, A. R., and Heasley, J. H. 1966. Extension of Darken's Equation to binary diffusion in ceramics. J. Amer. Ceram. Soc. 49(5):280-284.

Crank, J. 1956. Mathematics of diffusion. Clarendon Press, Oxford.

Curtis, C. E., Doney, L. M., and Johnson, J. R. 1954. Some properties of hafnium oxide, hafnium silicate, calcium hafnate, and hafnium carbide. J. Amer. Ceram. Soc. 37(10):458-465.

Darken, L. S. 1948. Diffusion, mobility and their interrelation through free energy in binary metallic systems. Trans. AIME 175:184-194.

Franklin, A. D. 1968. Born model calculation of defect energies in CaF_2. J. Phys. Chem. Solids 29:823-841.

Gessel, G. R. 1971. Interdiffusion in the polycrystalline systems Er_2O_3-Y_2O_3 and Er_2O_3-Ho_2O_3. M.S. Thesis. Iowa State University, Ames, Iowa.

Johnstone, J. K. 1970. The erbia-hafnia system. Ph.D. Thesis, Iowa State University, Ames, Iowa.

Macki, J. M. 1968. Electrical conductivity of pure and doped Dy_2O_3 and Gd_2O_3. Ph.D. Thesis. Ohio State University, Columbus, Ohio.

Matano, C. 1933. On the relation between diffusion coefficients and concentrations of solid metals (the nickel-copper system). Japanese J. Phys. 8(3):109-113.

Matzke, H. 1970. Fluorine self-diffusion in CaF_2 and BaF_2. J. Mater. Sci. 5(10):831-836.

Rhodes, W. H., and Carter, R. E. 1966. Cationic self-diffusion in calcia-stabilized zirconia. J. Amer. Ceram. Soc. 49(5):244-249.

Sauer, F., and Freise, V. 1962. Diffusion in binary mixtures with volume change. Z. Elektrochem. 66(4):353-363.

Scheidecker, R., and Berard, M. F. 1973. Interdiffusion in the system CaF_2-SrF_2. J. Amer. Ceram. Soc. 56(4):204-206.

Scheidecker, R., and Berard, M. F. 1976. Interdiffusion in SrF_2-BaF_2. Submitted to J. Amer. Ceram. Soc.

Schieltz, J. D., Patterson, J. W., and Wilder, D. R. 1971. Electrolytic behavior of yttria-stabilized hafnia. J. Electrochemical Soc.: Electrochemical Science 118(8): 1257-1261.

Simpson, L. A., and Carter, R. E. 1966. Oxygen exchange and diffusion in calcia-stabilized zirconia. J. Amer. Ceram. Soc. 49(3):139-144.

Visser, R. G., Schiavi, W. F., and Berard, M. F. 1975. Interdiffusion in the CaF_2-YF_3 system. J. Amer. Ceram. Soc. 58(9-10):438-441.

Wagner, C. 1969. The evaluation of data obtained with diffusion couples of binary single-phase and multiphase systems. Acta Met. 17(2):99-107.

Whitney, W. P., II, and Stubican, V. A. 1971. Interdiffusion studies in the system MgO-Al_2O_3. J. Phys. Chem. Solids 32:305-312.

ACKNOWLEDGEMENTS

The author gratefully acknowledges the assistance of Ceramic Engineering Groups I, II, and III of the Ames Laboratory, ERDA; C. D. Wirkus of the Engineering Research Institute, Iowa State University, who performed the electron microprobe analyses of the interdiffusion couples; and Miss Verna Thompson, who typed the manuscript. The author is especially grateful to Dr. M. F. Berard for his guidance and encouragement in the performance of the interdiffusion experiments and the preparation of this thesis.

APPENDIX

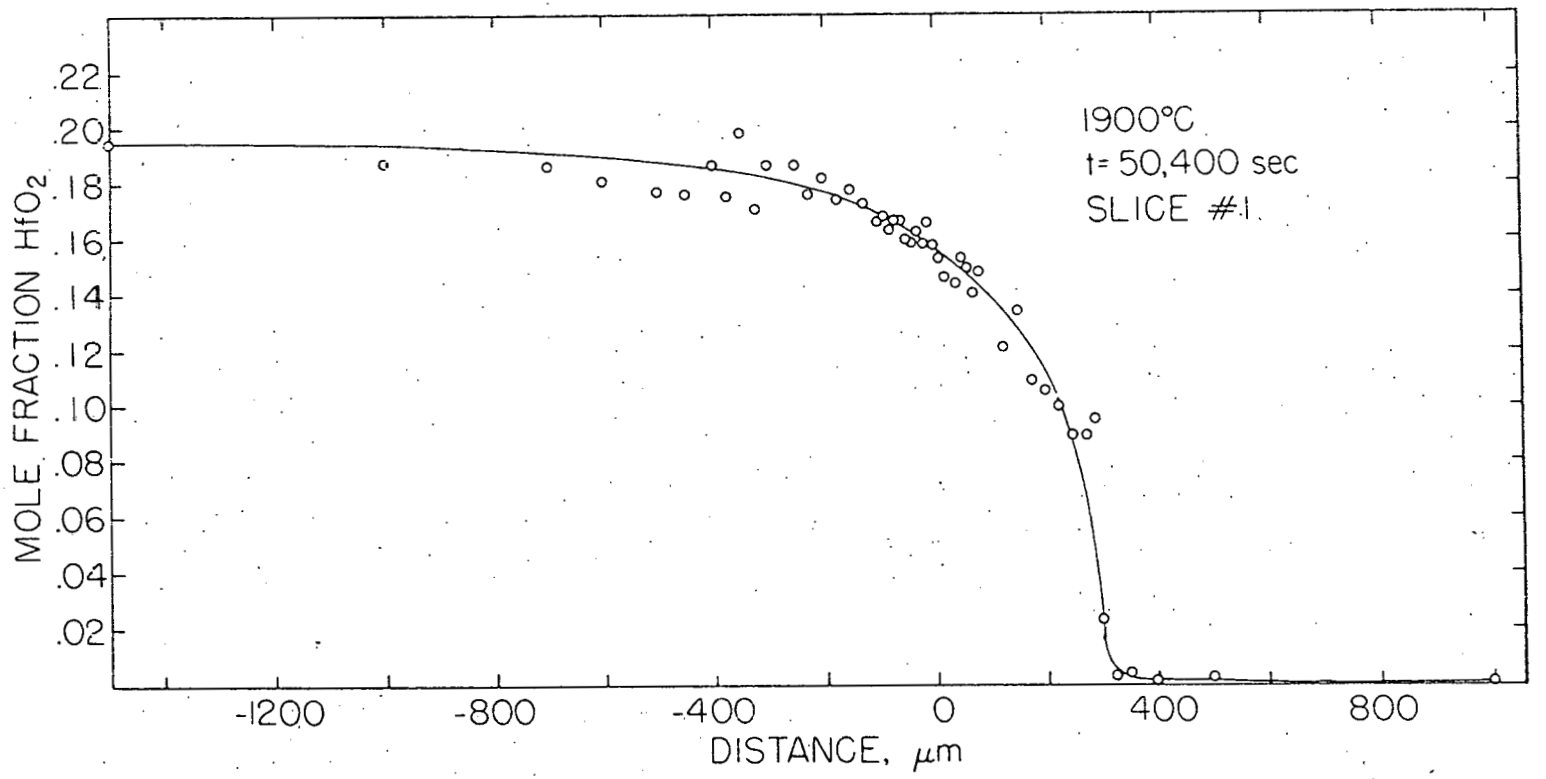

Figure A1. Interdiffusion composition profile

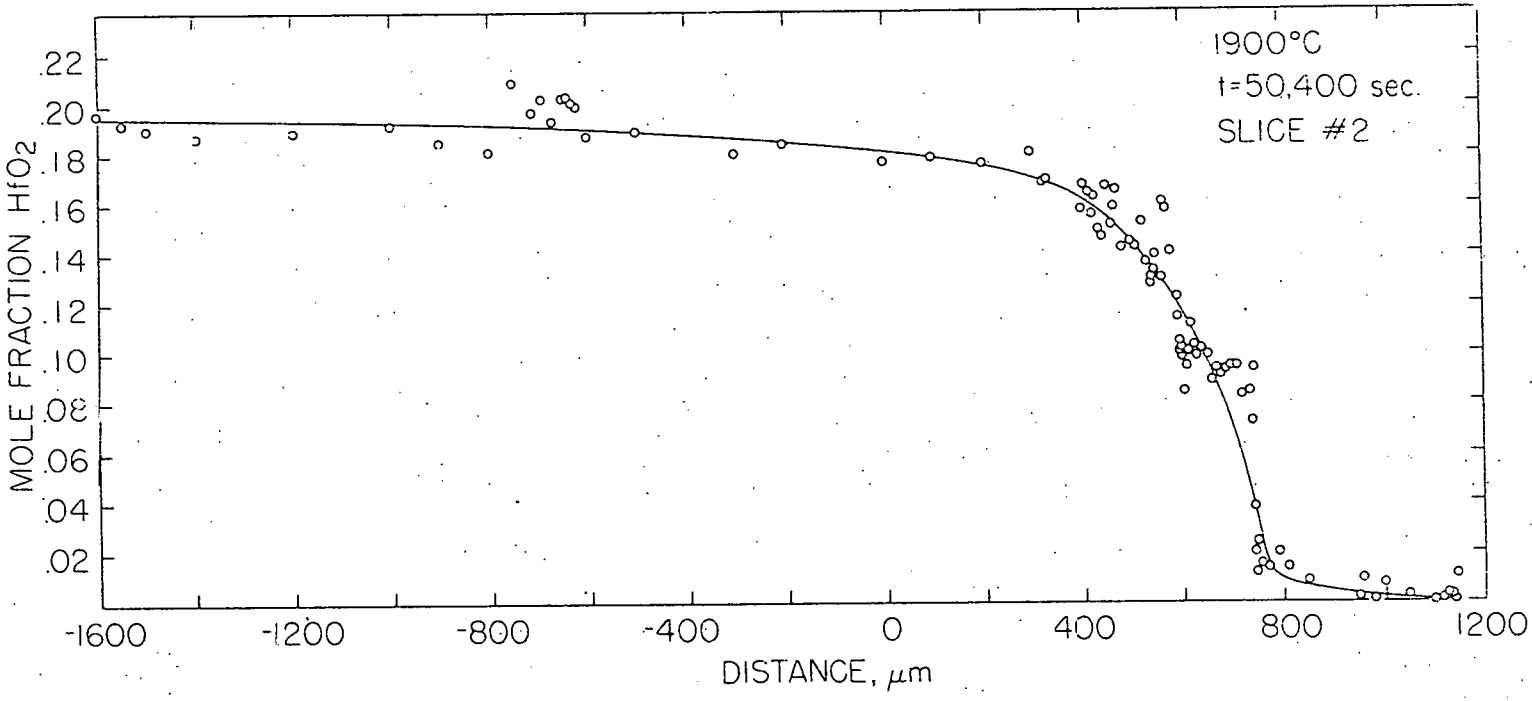

Figure A2. Interdiffusion composition profile

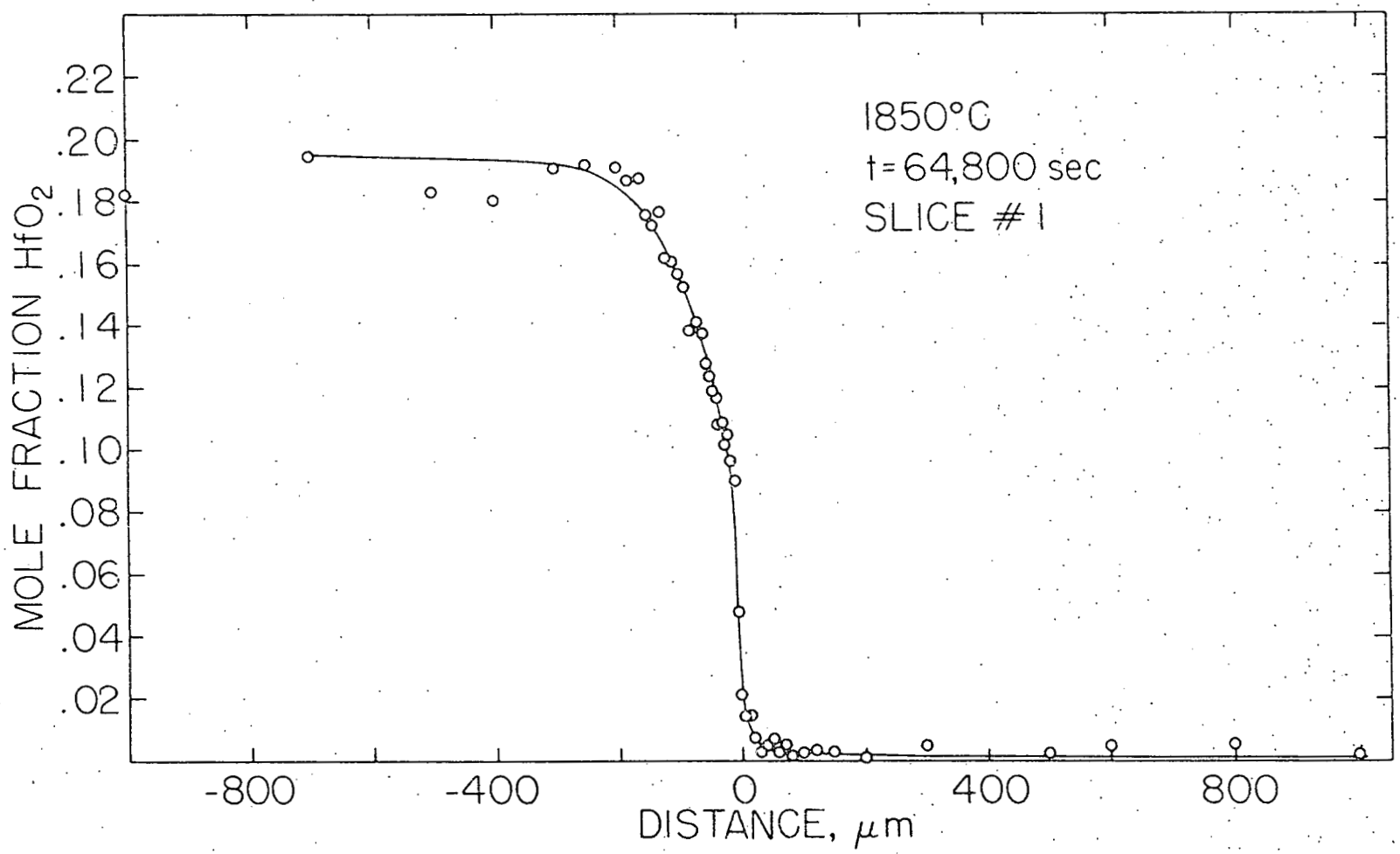

Figure A3. Interdiffusion composition profile

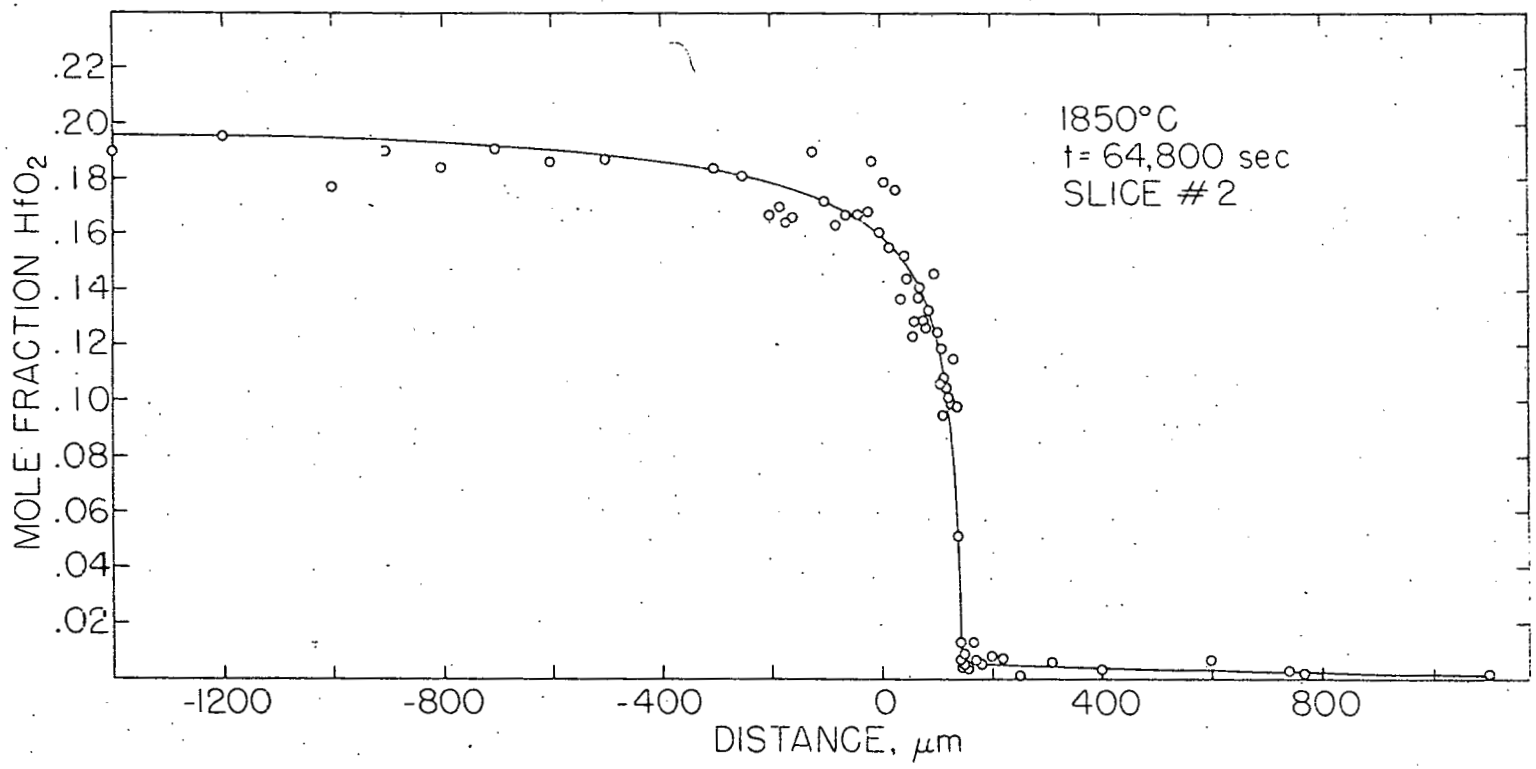

Figure A4. Interdiffusion composition profile

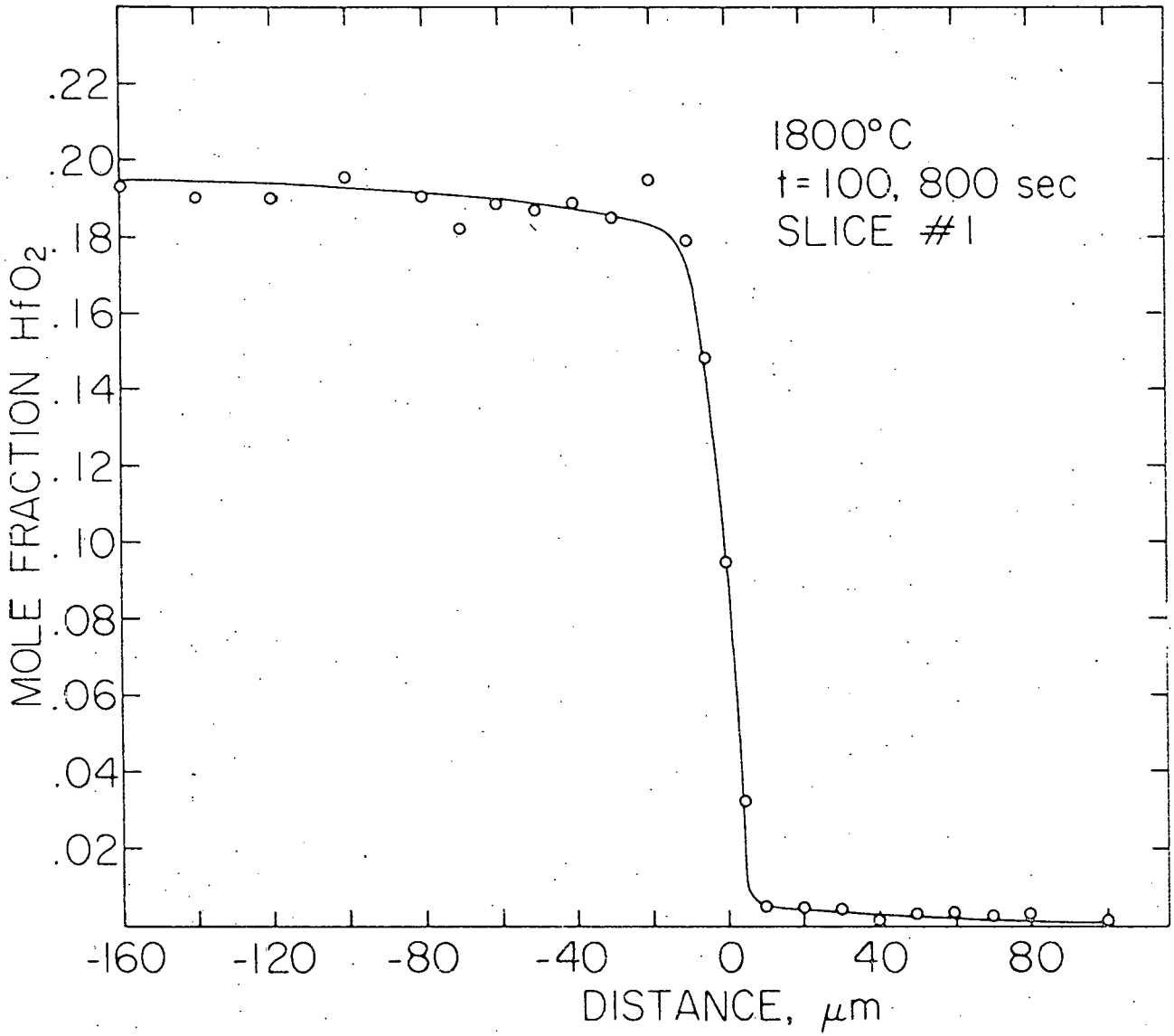

Figure A5. Interdiffusion composition profile

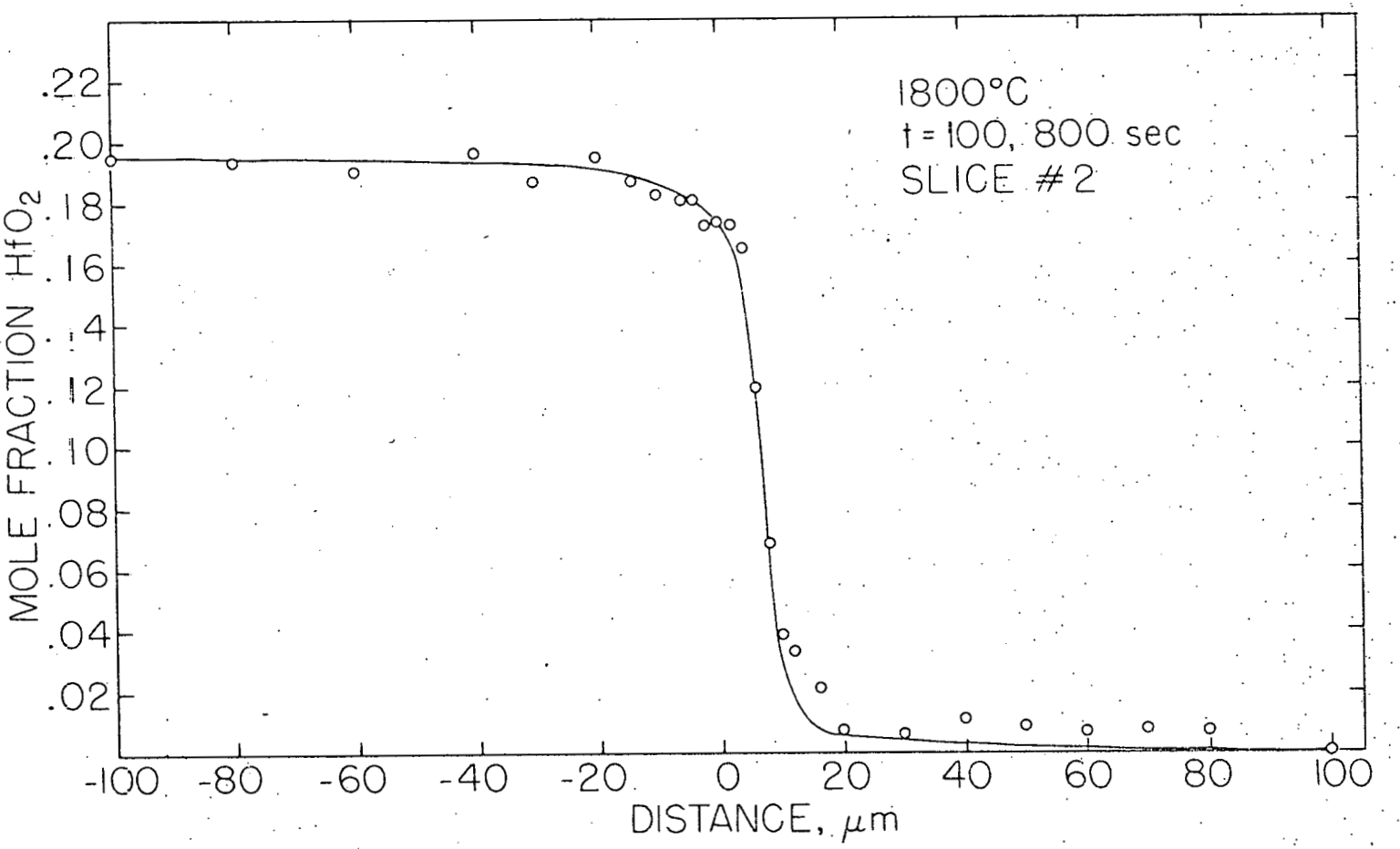

Figure A6. Interdiffusion composition profile

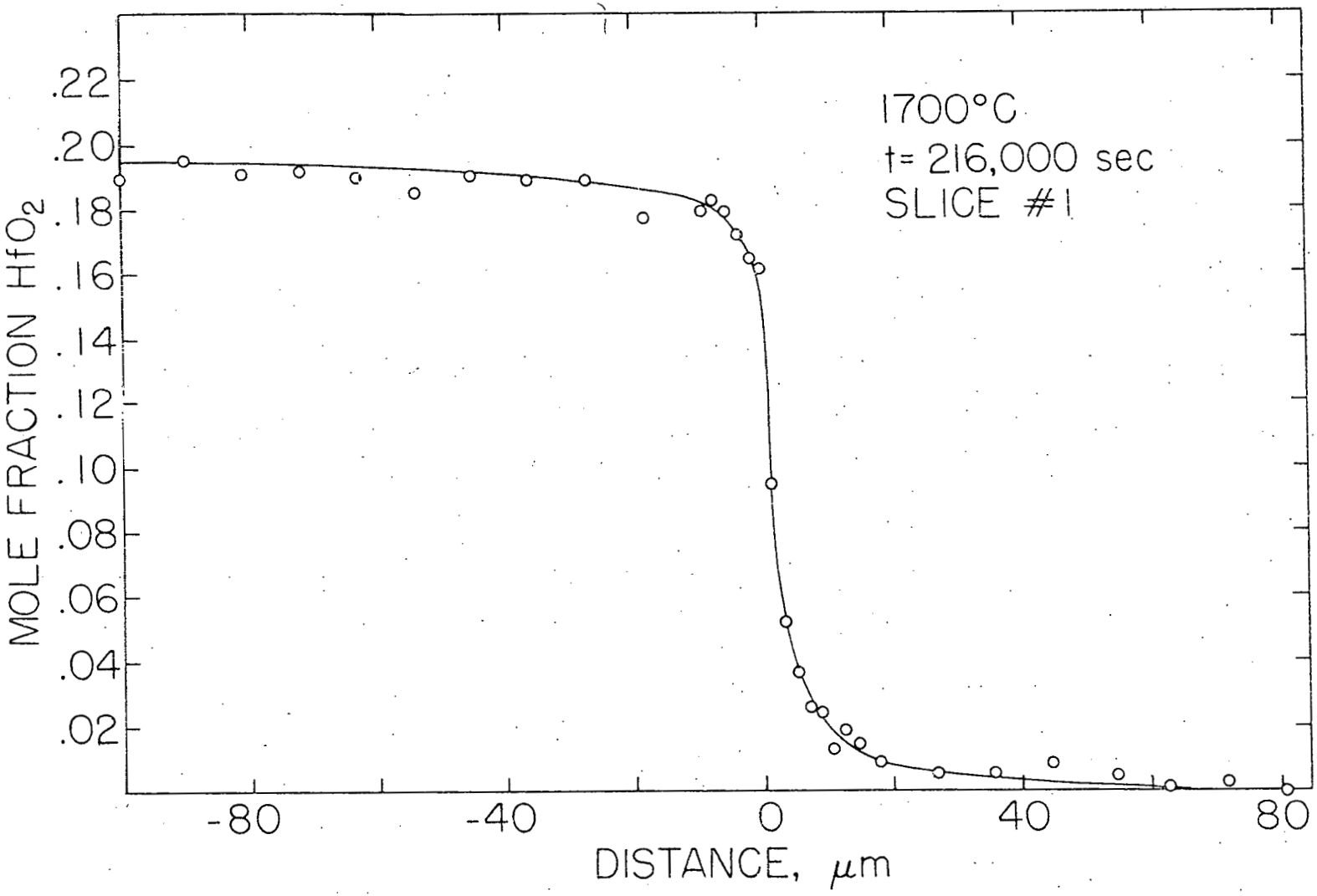

Figure A7. Interdiffusion composition profile

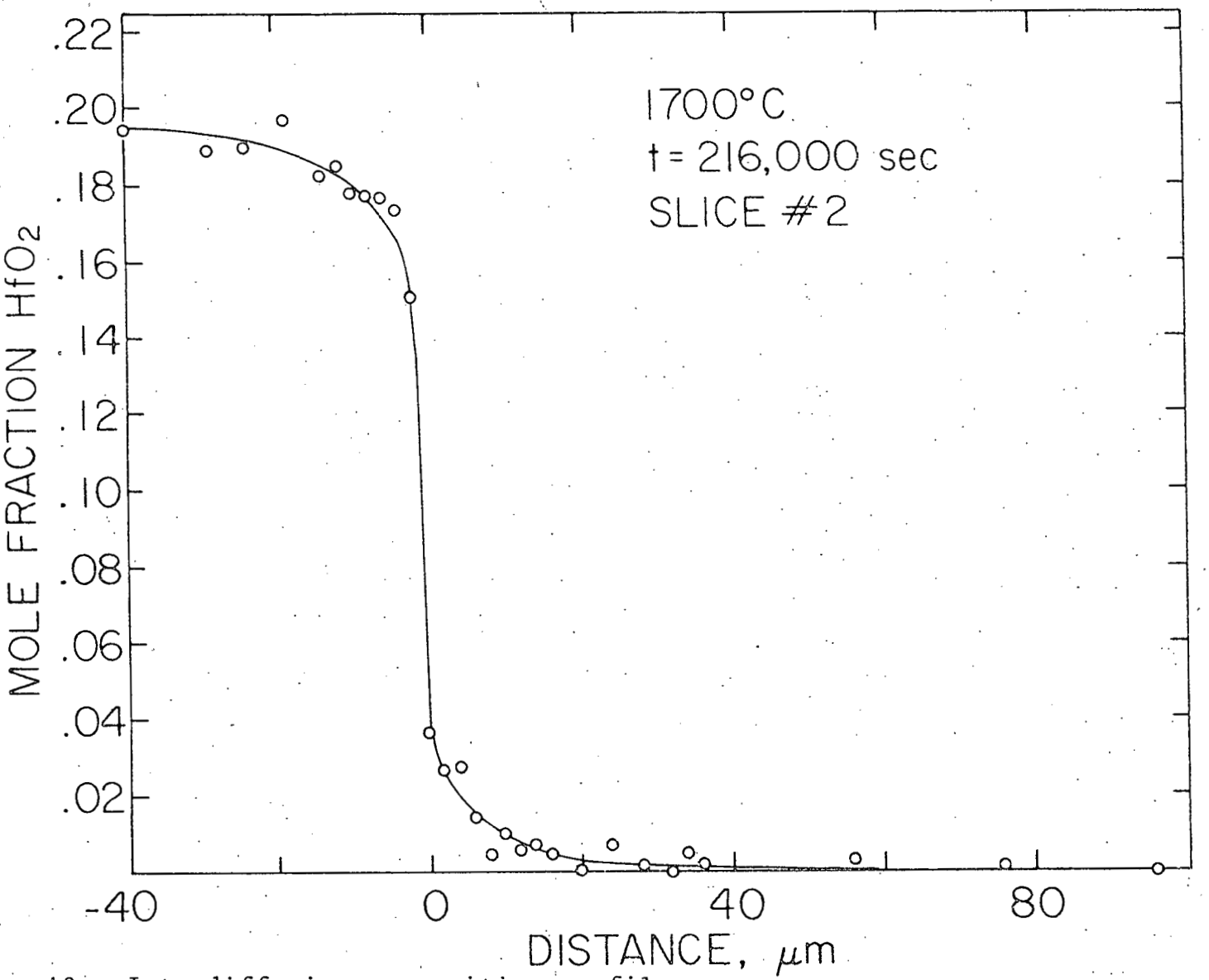

Figure A8. Interdiffusion composition profile

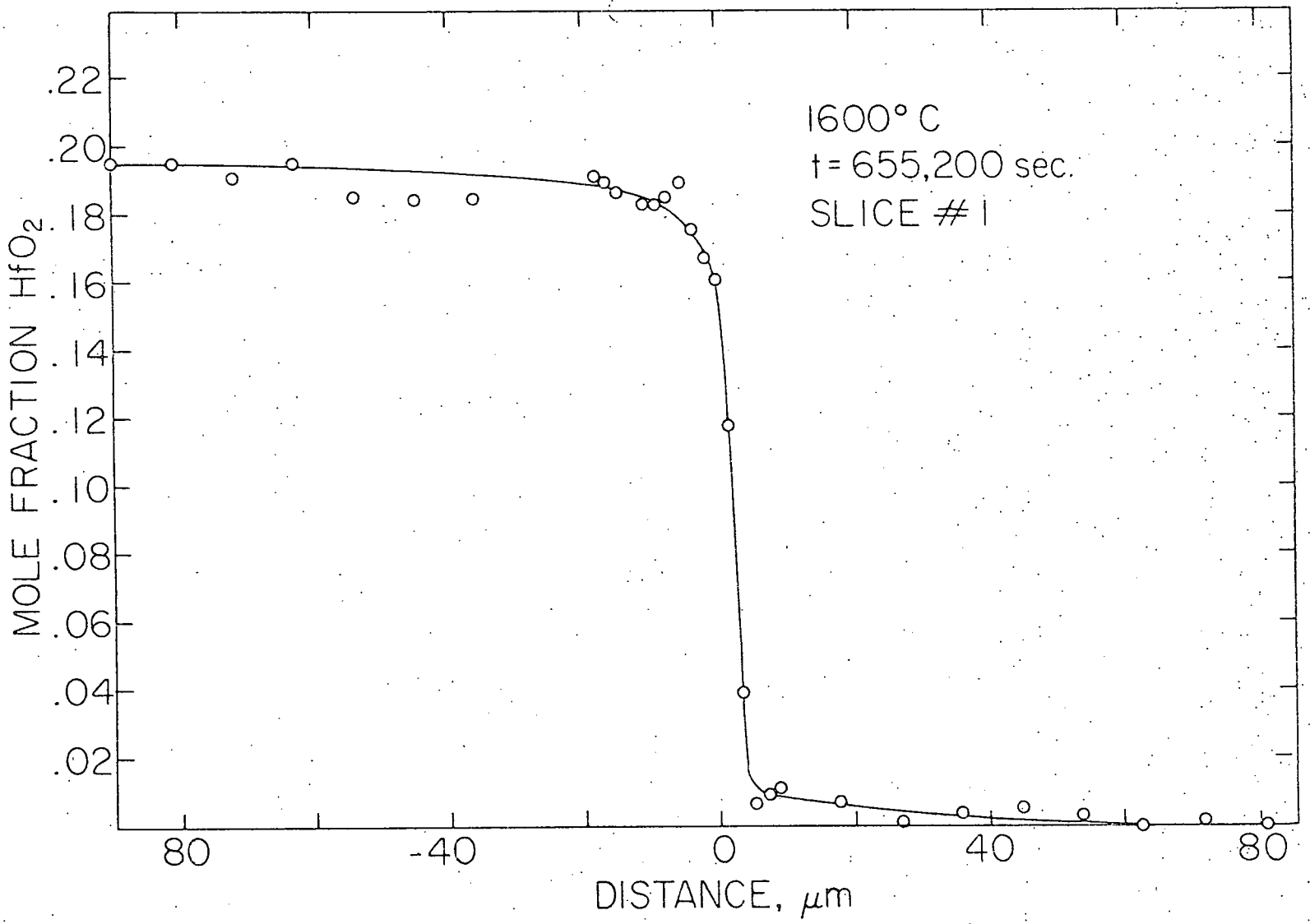

Figure A9. Interdiffusion composition profile

Table A1. Experimental interdiffusion coefficients, 1900°C

N_{HfO_2}	$\tilde{D}$, cm^2/sec	
	Slice #1	Slice #2
.19	5.38×10^{-8}	8.80×10^{-8}
.18	1.92×10^{-8}	6.87×10^{-8}
.16	1.11×10^{-8}	1.56×10^{-8}
.14	8.60×10^{-9}	8.67×10^{-9}
.12	4.01×10^{-9}	7.43×10^{-9}
.10	2.59×10^{-9}	4.88×10^{-9}
.08	1.55×10^{-9}	3.17×10^{-9}
.06	9.06×10^{-10}	2.09×10^{-9}
.04	4.41×10^{-10}	1.26×10^{-9}
.02	2.71×10^{-10}	5.63×10^{-10}
.01	4.80×10^{-10}	2.68×10^{-9}
.005	5.90×10^{-10}	5.93×10^{-9}

Table A2. Experimental interdiffusion coefficients, 1850°C

N_{HfO_2}	$\tilde{D}$, cm^2/sec	
	Slice #1	Slice #2
.19	1.86×10^{-9}	2.08×10^{-8}
.18	1.05×10^{-9}	1.22×10^{-8}
.16	9.10×10^{-10}	5.10×10^{-9}
.14	6.82×10^{-10}	2.00×10^{-9}
.12	5.80×10^{-10}	9.97×10^{-10}
.10	5.02×10^{-10}	5.82×10^{-10}
.08	1.18×10^{-10}	3.01×10^{-10}
.06	2.93×10^{-11}	1.55×10^{-10}
.04	1.46×10^{-11}	7.24×10^{-11}
.02	1.25×10^{-10}	2.79×10^{-11}
.01	2.05×10^{-10}	2.15×10^{-11}
.005	7.90×10^{-10}	9.72×10^{-9}

Table A3. Experimental interdiffusion coefficients, 1800°C

N_{HfO_2}	$\tilde{D}$, cm^2/sec	
	Slice #1	Slice #2
.19	2.83×10^{-10}	3.13×10^{-11}
.18	4.48×10^{-11}	1.22×10^{-11}
.16	7.10×10^{-12}	3.29×10^{-12}
.14	5.56×10^{-12}	1.28×10^{-12}
.12	5.51×10^{-12}	1.14×10^{-12}
.10	3.91×10^{-12}	9.51×10^{-13}
.08	3.47×10^{-12}	8.46×10^{-13}
.06	2.21×10^{-12}	5.75×10^{-13}
.04	1.29×10^{-12}	1.07×10^{-12}
.02	7.23×10^{-13}	3.14×10^{-12}
.01	2.93×10^{-12}	6.60×10^{-12}
.005	2.05×10^{-10}	5.44×10^{-11}

Table A4. Experimental interdiffusion coefficients, 1700°C

N_{HfO_2}	$\tilde{D}$, cm^2/sec	
	Slice #1	Slice #2
.19	4.75×10^{-11}	5.59×10^{-12}
.18	9.32×10^{-12}	3.99×10^{-12}
.16	1.50×10^{-12}	1.31×10^{-12}
.14	3.99×10^{-13}	3.04×10^{-13}
.12	3.46×10^{-13}	1.38×10^{-13}
.10	2.16×10^{-13}	9.78×10^{-14}
.08	4.89×10^{-13}	9.36×10^{-14}
.06	1.21×10^{-12}	1.14×10^{-13}
.04	2.19×10^{-12}	1.91×10^{-13}
.02	4.44×10^{-12}	2.50×10^{-12}
.01	8.47×10^{-12}	4.09×10^{-12}
.005	3.20×10^{-11}	6.07×10^{-12}

Table A5. Experimental interdiffusion coefficients, 1600°C

N_{HfO_2}	$\tilde{D}$, cm^2/sec
.19	9.31×10^{-12}
.18	1.83×10^{-12}
.16	3.37×10^{-13}
.14	1.21×10^{-13}
.12	9.94×10^{-14}
.10	9.05×10^{-14}
.08	8.48×10^{-14}
.06	6.28×10^{-14}
.04	5.27×10^{-14}
.02	7.61×10^{-14}
.01	1.53×10^{-12}
.005	6.76×10^{-12}